Quantum dots on bilayer graphene made on a substrate of boron nitride using split gates

T.A. Baart

February 2011

Master Thesis
Supervisors: prof. dr. ir. L.M.K. Vandersypen and drs. A.M. Goossens
Delft University of Technology
Faculty of Applied Sciences
Quantum Transport group

Abstract

In this project a method has been developed to fabricate the device structure for a quantum dot on bilayer graphene made on a boron nitride substrate. Quantum dots in bilayer graphene give us the ability to study the special properties of electrons inside this material; including a gapless electron-hole crossover and a fourfold degeneracy of electrons. The usage of boron nitride as a substrate instead of the usual SiO_2 should help us improve the quality of our devices. In the future we hope to create a qubit for quantum information processing with lower decoherence times as compared to conventional dots (e.g. GaAs). Measurements have been performed on an intermediate device in which the graphene flake was not yet fully surrounded by boron nitride as dielectric. This device used boron nitride as backgate dielectric and silicon oxide for the top gates. These measurements show that it is possible to influence the doping of the graphene with the gates, but we have not yet been able to demonstrate the full functionality of bilayer graphene; such as the opening of a bandgap. This report will describe the method to make the devices (fully using boron nitride as a dielectric), recommendations are given on how to improve the quality and future experiments are discussed.

Contents

Chapter 1

Introduction: quantum dots in bilayer graphene

The ongoing miniaturization of solid state devices has led to a.o. the development of quantum dots (QD's). Quantum dots are small regions defined in a semiconductor material with a size of order 100 nm. Since the first studies in the late eighties, the physics of quantum dots has been a very active and fruitful research topic. Topics such as the physics of artificial atoms, coupled quantum systems and the quantum Hall effect have been studied.
A quantum dot is made out of roughly a million atoms with an equivalent number of electrons. Almost all electrons in the dot are tightly bound to the nuclei of the material, only a few (between one and a hundred) are free. The de Broglie-wavelength of these free electrons is comparable to the size of the dot, due to which the electrons occupy discrete energy levels and have a discrete excitation spectrum. A quantum dot has another characteristic called the charging energy; this is the energy required to add or remove a single electron from the dot [1]. The ability to control current through these dots at the single-electron level make it an interesting object. A future application would be the usage of a dot for quantum information processing (QIP). QIP can solve certain computational problems in a more efficient way than classical computers (e.g. Shor's algorithm), and can give us the ability to simulate quantum systems and better understand for example high-T_c superconductivity. QIP requires quantum bits (qubits) which can be made 'inside' quantum dots. A quantum dot allows us to 'capture' one electron inside a specific region in space and manipulate its properties (such as its spin). By this manipulation we can for example put the electron in a superposition and thereby create a qubit.
So far nothing has been said about what material to use for the quantum dot. They have been made in for example GaAs/AlGaAs 2DEG's and in nanowires. At this moment bilayer graphene is an interesting candidate. Bilayer graphene is a two atom thick sheet of carbon atoms with unusual electronic properties, a.o. high electron mobilities, low spin-orbit coupling and a tunable bandgap. These properties make it a high potential candidate for applications in nanoelectronics. This project will focus specifically on building of a quantum dot in bilayer graphene. This is interesting for two reasons:

1. QIP requires long decoherence times of the quantum dots. Due to the low spin-orbit coupling and hyperfine interaction in graphene, it is expected that the decoherence rates will be low inside graphene quantum dots.

2. The (special) behaviour of confined electrons in graphene can be studied. Next to the usual spin degeneracy, charge carriers in graphene also have valley degeneracy leading to a total fourfold degeneracy. Also, the bandgap of graphene inside the dot will be (close to) zero. This makes it experimentally possible to change the charge carriers from electrons to holes or vice versa. In conventional GaAs dots the electron-hole crossover spans an energy range of $\sim$1 eV which is too large for standard experimental circumstances.

To create a quantum dot in graphene several processing steps need to be performed including the creation of graphene using mechanical exfoliation [2], the transfer of graphene to a suitable substrate, annealing the substrates and writing of the electrodes plus top gates. A schematic overview of the device is shown in Fig. 1.1.

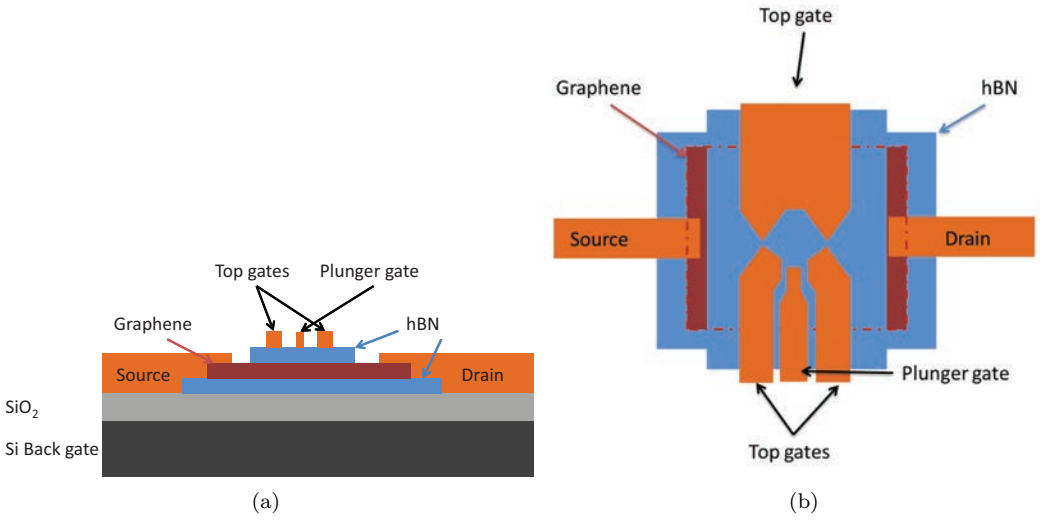

Figure 1.1: Schematics of the device structure (not to scale); (a) side view, (b) top view.

Thus far graphene systems show lower quality than expected [3]. This is primarily seen from the fact that the measured mobilities are quite low due to a.o. (charged) impurities and surface roughness of the underlying substrate. As a result, the electron's mean free path is small and quantum dots tend to break up into several smaller dots. The usage of a different substrate, boron nitride, from the usual silicon oxide should improve the quality. As both the boron nitride flakes and the graphene flakes are only several micron large, it will not be possible to directly apply mechanical exfoliation of graphene on top of the boron nitride: the chance of the two aligning will be low. Therefore a transfer process needs to be developed to align the graphene on the substrate.

At the same time, a new way of setting the quantum dot's edges will be implemented. Up till now these edges have been made by relatively 'crude ways' of setting the boundaries, for example by etching away the unwanted pieces of graphene. These discontinuous boundaries give rise to unwanted edge states and scattering effects. It turns out that a bandgap can be opened in bilayer graphene by applying an electric field. This allows us to set the boundaries of the quantum dot by writing top gates on those locations, which in combination with the Si-backgate will create an electric field and shut off electronic transport. The opening of a bandgap is not possible in a monolayer, which motivates our choice for bilayer graphene.

This project has focussed on (1) the so-called 'dry transfer method', (2) the use of the substrate hexagonal boron nitride (hBN) instead of the usual silicon oxide and (3) the influence of annealing the samples. Specific details of these steps will be described including ways to optimize the results. At the moment of writing this report we have succeeded in creating a device such as shown in Fig. 1.1, but it has not yet been possible to perform the first measurements; these will be done in the coming weeks. In the mean time a device with the top hBN-flake absent, but SiO_2 underneath the top gates (only under the gates, not on the other parts of graphene) has also been made and some first measurements have just been performed.

1.1 Outline of this thesis

This report presents a method for making quantum dots of bilayer graphene on boron nitride substrates, followed by some first measurements of an almost similar device with the top hBN-flake replaced locally with SiO_2.
Chapter 2 will give the formal basis for the promises made in this introduction. It introduces the reader to the basics of graphene, quantum dots and Raman spectroscopy measurements. It also explains why boron nitride has been chosen as a replacement for silicon oxide and should lead to higher quality devices. This chapter concludes with estimations for the relevant energy scales inside the quantum dot and discusses what measurements need to be done.
Chapter 3 explains the details of the dry-transfer method, ranging from finding the graphene and boron nitride to writing the gate structures.
Chapter 4 demonstrates for which annealing settings the sample quality improves and contains a small experiment concerning the nature of the bubbles that form on graphene sheets.
Chapter 5 contains an overview of the experimental setup and shows measurement results of a device using SiO_2 instead of hBN as dielectric for the topgates.
Chapter 6 summarizes the results and contains recommendations to extend this line of research.

This research has been performed starting halfway September 2010 until the end of February 2011 as part of my second 'master rotation' for the Casimir pre-PhD track.

Chapter 2

Theoretical background

2.1 Bandstructure of bilayer graphene

The band structure of graphene has already been described by P.R. Wallace in 1946 [4]. At that time Landau and Peierls argued that strictly 2D crystals were thermodynamically unstable and could not exist [5, 6]. However, in 2004 Novoselov et al. [2] realized the experimental discovery of graphene. We will now briefly describe the bandstructure of bilayer graphene and demonstrate how it can be used to open a bandgap (needed to set the boundaries of the QD).

In Fig. 2.1 the honey comb lattice structure of bilayer graphene with Bernal stacking is illustrated. A unit cell contains four atoms: A, B from the top layer and A', B' from the bottom layer. As a result the dispersion of bilayer graphene contains four bands. The lattice sites B sit exactly on top of A' lattice sites and form the nearest neighbours between the layers.
Each carbon atom has four valence electrons and three of these are used for the formation of sp^2 hybridization orbitals which form three σ bonds with the neighbouring atoms. The fourth electron occupies the p_z orbital which is perpendicular to the graphene plane. It overlaps with neighbouring p_z-electrons to form π bonds. The p_z electrons are delocalized over the entire lattice and will form the main contribution to electronic transport. By applying the tight binding model to these p_z-electrons the following dispersion relation is found [7–9]:

$$E_{\pm}^2(p) = v_F^2 p^2 + \gamma_1^2/2 + V^2/4 \pm \sqrt{\gamma_1^4/4 + (\gamma_1^2 + V^2)\, v_F^2 p^2} \tag{2.1}$$

where γ_1 denotes the overlap integral between A' and B (see Fig. 2.1 (b)), V the potential difference between the two sublattices A' and B, and v_F is the Fermi velocity ($\approx 10^6$ m/s). For our experiments the black and blue energyband as shown in Fig. 2.2 will be of importance, the other two bands will be out of the used energy range.
For this project one final note can be made about the bandstructure: two sets of electrons at different points in reciprocal space (K- and K'-valleys) have the same dispersion relation, giving rise to valley degeneracy. This implies that besides spin degeneracy, electrons also have valley degeneracy which leads to a total fourfold degeneracy [10].

By applying a perpendicular electric field to a bilayer graphene sheet a bandgap can be opened by the V-term described in Eq. 2.1 which is shown in Fig. 2.2. The bandgap $E_g = \sqrt{V^2\gamma_1^2/(V^2+\gamma_1^2)}$ is slightly smaller than V for $V \ll \gamma_1$. Experimental verification of this principle has been demonstrated in [12]. We follow the same strategy as in [12] to make our QD's. This allows us to set the boundaries of the QD using the combination of a back- and topgate.

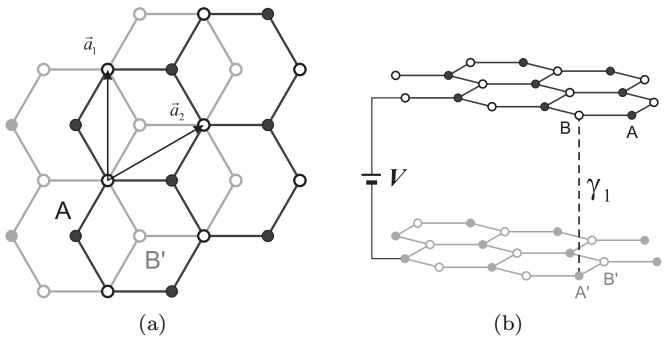

Figure 2.1: Illustrations of the lattice structure of bilayer graphene: (a) top view, (b) 3D view [11].

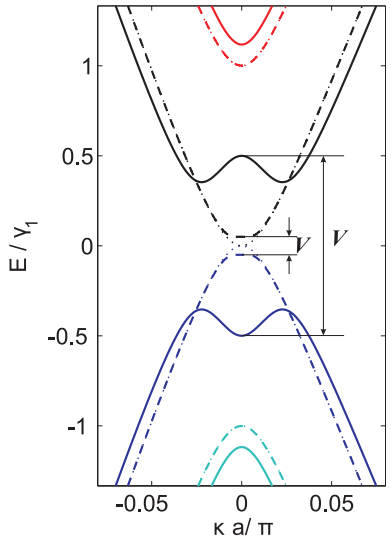

Figure 2.2: The band structure of graphene around the K point calculated using $\gamma_1 = 0.1t \approx 0.3$ eV, $V = \gamma_1$ (solid lines), $V = 0.1\gamma_1$ (dashed lines), and $V = 0$ (thin dotted lines) [11].

2.2 Quantum dots

When a device such as shown in Fig. 1.1 has been made, a QD can be created by applying suitable back- and topgate voltages. These gates should be tuned in such a way that a bandgap is opened at the position of the top gates, and that the Fermi-level is put inside the bandgap to make that piece of graphene non-conducting. The bandgap can be opened by creating a voltage *difference* between the top- and backgate. And the Fermi-level can be changed by the *sum* of the two voltages. To be more precise: $n = C_{\text{top gate}}V_{\text{top gate}} + C_{\text{back gate}}V_{\text{back gate}}$[1] where C is the respective capacitance (more on that in section 2.5) and n the doping which should go to zero to get the Fermi-level inside the gap.
If we get these conditions right and look at Fig. 1.1 (b), we see that the structure of the top gates and the plunger gate will form barriers through which electrons should not be able to go through. Next to that, there are two constrictions left and right for the electrons to leave or enter the island between the gates. If the properties of the device are good enough, i.e. high enough mobili-

[1] In practice this formula also contains an offset for both the top- and backgate, but for the present discussion that won't be necessary.

ties and not too much variation in the doping over the graphene flake, this island will become a QD.

This section will cover the basic theory of QD's, discuss the special properties that graphene quantum dots should show in comparison to 'conventional quantum dots' (such as GaAs) and conclude with a short overview of other known methods to create QD's in graphene.

2.2.1 Basic theory of quantum dots

A schematic overview of our QD is shown in Fig. 2.3 (a). The island/dot is connected to the source (S) and drain (D) contacts via two tunnel barriers (i.e. $R_{barrier} \gg h/e^2$). The two tunnel barriers have been formed by the small constrictions between the topgates (TG) (NB: the constriction between the plunger gate (PG) and neighbouring top gates should be so small that almost no electrons leak out from there). The plunger gate and backgate (BG) couple capacitively to the electron levels in the dot which allows their energy levels to be controlled. Fig. 2.3 (b) depicts a schematic in terms of capacitances and resistances.

Fig. 2.4 (a) shows the potential landscape of the QD along the transport direction. The states in the leads are filled up to the electrochemical potentials μ_S and μ_D which are governed by the externally applied source-drain voltage ($V_{SD} = (\mu_S - \mu_D)/e$). The chemical potential in the dot, μ_{dot} is defined as the minimum energy for adding the Nth electron to the dot: $\mu_{dot} \equiv U(N) - U(N-1)$ where $U(N)$ is the total ground state energy for N electrons on the dot at zero temperature. $U(N)$ can be calculated quite easily by making the following assumptions: (1) the quantum levels can be calculated independently of the number of electrons on the dot, (2) interaction among the electrons in the dot and between electrons in the dot and those elsewhere the environment (as in the metallic gates) are described by a constant capacitance C, (3) this value C is independent of the number of electrons on the dot. For our device the total capacitance C is given by $C = C_S + C_D + C_{BG} + C_{TG} + C_{PG} + C_{\text{self capacitance}}$. All capacitance values are determined by the geometry and material of each capacitor (see section 2.5 for calculations). Using these assumptions one arrives at the following formula for $U(N)$:

$$U(N) = \frac{(-e(N-N_0) + C_S V_S + C_D V_D + C_{BG} V_{BG} + C_{TG} V_{TG} + C_{PG} V_{PG})^2}{2C} + \sum_{n=1}^{N} E_n \quad (2.2)$$

The first term describes the electrostatic energy; E_n represents the single particle energy-levels and N_0 represents the number at zero gate voltage. Using this formula we find:

$$\mu_{dot}(N) = U(N) - U(N-1) =$$
$$(N - N_0 - \frac{1}{2})E_c - \frac{E_c}{e}(C_S V_S + C_D V_D + C_{BG} V_{BG} + C_{TG} V_{TG} + C_{PG} V_{PG}) + E_N \quad (2.3)$$

where $E_c = e^2/C$ is defined as the charging energy of the dot [1]. The energy to add one electron to the dot, the addition energy E_a, becomes:

$$E_a = \mu_{dot}(N+1) - \mu_{dot}(N) = E_c + E_{N+1} - E_N \quad (2.4)$$

The spacing between two charge states therefore includes two contributions: E_c for the electrostatic interaction and $E_{N+1} - E_N$ from confinement. This nonzero addition energy can lead to a blockade for tunnelling on and off the dot as depicted in Fig. 2.4 (a). If the number of available states in the energy window between μ_S and μ_D is zero, electrons cannot tunnel on the dot as the resulting μ_{dot} would be higher than the potentials of the reservoirs. For $\mu_{dot}(N) < \mu_S, \mu_D < \mu_{dot}(N+1)$ the electron transport is blocked, which is known as Coulomb blockade.

Coulomb blockade is typically measured by making a plot of the differential conductance versus V_{Bias} and V_{PG}: this will reveal regions with zero differential conductance; the so-called Coulomb diamond (see Fig. 2.4 (b)). The transport is blocked inside the grey diamonds. Values of N depict

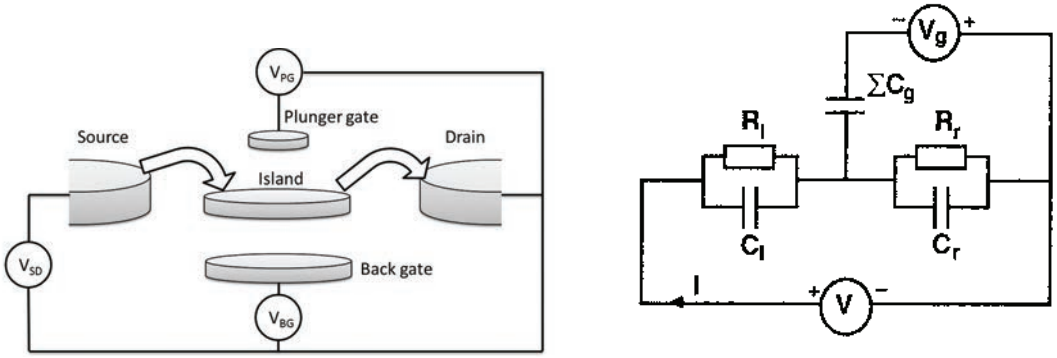

(a) (b)

Figure 2.3: (a) Schematic of a QD, in the shape of a disk, connected to source and drain contacts by tunnel junctions and to a back- and plungergate by a capacitor. (b) Electronic circuit in which the source/drain are represented as a parallel capacitor and resistor. The different gates are represented by a single capacitor. [1]

the amount of excess electrons inside the QD. The height of the diamonds is given by E_C, the width depends on the coupling of the PG with the dot. If the level spacing $E_{N+1} - E_N$ lies within a measurable range, it will show up as lines of non-zero conductance parallel to the edges of the diamonds.
When the V_{PG} shifts the Fermi level through the bandgap/Dirac point of the graphene, the system will switch from electrons to holes (or vice versa). The bandgap determines the height and width of this specific $N = 0$ diamond. The ability to set up a quantum dot in a state with a predetermined number of only a few electrons or holes might be extremely important for the realization of a particular spin state and thus for the implementation of qubits [13].

2.2.2 Special properties of graphene quantum dots in comparison to 'conventional' quantum dots

Measurements on QDs have already been performed since the late eighties on various materials such as GaAs/AlGaAs and CdSe [1, 15]. This section will discuss what differences we expect between those 'conventional dots' and our graphene dots and will form a further motivation for our choice for graphene.

- Carbon-based materials lead to less decoherence for two reasons: (1) due to carbon's relatively low atomic weight spin-orbit coupling is weak, (2) 99% of natural carbon consists of the zero-spin isotope C-12 for which hyperfine interaction is absent (in GaAs all atoms have spin 1). [16].

- Electron states in graphene are fourfold degenerate (instead of the usual 2 in GaAs), see section 2.1. This implies that the addition energy (Eq. 2.4) should be constant, i.e. $\frac{e^2}{C}$ for every three electrons added, then increases by $E_{N+1} - E_N$ for the fourth electron and will be constant again ($\frac{e^2}{C}$) for the next three electrons. This would imply that every fourth Coulomb diamond from Fig. 2.4 is somewhat larger (the height should increase by $E_{N+1} - E_N$ w.r.t the other diamonds).

- The bandgap of graphene inside the dot will be small (it should be approximately zero) compared to the bandgap of dots such as GaAs/AlGaAs (∼1.4-2.2 eV [17]). The large

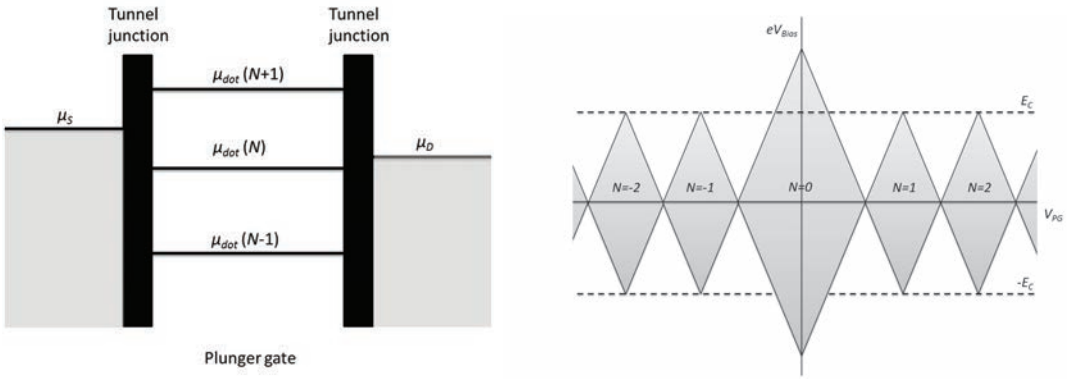

(a) (b)

Figure 2.4: (a) Potential landscape of a quantum dot depicting an example of Coulomb blockade. By tuning the V_{PG} one can shift the Fermi level inside the dot and thereby the position of these levels. By applying a source-drain voltage one shifts the relative position of the chemical potential left and right of the dot; when these align with the levels inside the dot conductance is possible again. (b) Coulomb diamonds in a graphene QD; the transport is blocked inside the grey diamonds. Values of N depict the amount of excess electrons inside the QD. When the V_{PG} shifts the Fermi level through the bandgap of the graphene the system will switch from electrons to holes (or vice versa). [1, 14]

bandgap of GaAs made it practically impossible to sweep the gate voltages over a wide enough range to perform electron-hole crossover; this is however possible now for graphene and has also been experimentally verified in [13]. The height/width of the Coulomb diamond at the position of the e-h crossover is determined by the sum of the local bandgap of the graphene and the usual addition energy. This principle allows is to empty a dot and precisely dictate the amount of electrons/holes in the QD.

2.2.3 Other known experimental setups to create quantum dots in graphene

At this moment three other techniques have been used to create quantum dots in (single layer) graphene. All techniques involve manipulating a sheet of graphene in such a way that its boundaries are changed into the shape of the desired dot. Method (1) involves the etching of the graphene flake [18], method (2) relies upon the controlled rupture of a suspended graphene sheet subject to a large electron current [19] and method (3) applies local cutting of a biased conductive tip of an atomic force microscope (AFM) [13]. All these methods induce sharp discontinuities in the potential landscape at the edges of the dot, which will lead to more scattering of the charge carriers and possibly destroy ballistic transport properties [20]. The edges will also give rise to edge states with energies close to the Dirac point [21]. Their density of states is very high in a small energy window leading to small level spacing. This will make it more difficult to control single electrons in the dot close to the Dirac point, as it can switch more easily between different states. The method described in this thesis will lead to a smoother potential landscape by the gates, thereby increasing the chances for ballistic transport.

One can think of a fourth method to produce QD's in graphene that would involve suspended graphene. Mobilities of 200,000 $cm^2V^{-1}s^{-1}$ have been reported [22] which should make it a promising candidate for a dot. However, the electrostatic attraction between the graphene and the topgates is so large, that the graphene attaches to the (also suspended) topgates and thereby loses its functionality [23].

2.3 Hexagonal boron nitride as a substrate

Part of this project concerns the application of a different substrate than the usual silicon oxide: hexagonal boron nitride. This section will motivate our choice for hBN and explain some of its properties.

hBN has a lattice constant similar to that of graphite (interlayer distance: 3.3 versus 3.4 Å; bond length of 1.44 versus 1.42 Å [24]) and a large electrical bandgap (5.97 eV [25]). The dielectric properties of hBN compare favourably with SiO_2 ($\epsilon \approx 4$, $V_{\text{breakdown}} \approx 0.8\text{nm}^{-1}$), allowing the use of hBN as an alternative gate dielectric [26]. hBN has several advantages in comparison to SiO_2:

- The surface of SiO_2 is rougher than that of hBN, which is atomically flat. Surface roughness in the underlying substrate of graphene might induce surface ripples in the graphene which can lead to extra long range scattering effects due to local changes in the band structure.
- Owing to the strong, in-plane, ionic bonding of the planar hexagonal lattice structure, hBN is relatively inert and is expected to be free of dangling bonds or surface charge traps [3]. Therefore hBN is expected to contain less charged impurities than SiO_2 (see discussion below of [27]). These charged impurities will influence the local doping of the graphene and thereby locally the type of carriers. If the type of carriers varies within the dot, the dot will break up into multiple dots: something that should really be prevented in order to study the behaviour of a single dot. Furthermore, the charged impurities will induce more long range scattering and thereby decrease the mean free path of the electrons.
- hBN has twice as large optical phonon modes compared to SiO_2 [28, 29]; this will reduce the amount of scattering with these modes.

In August 2010 [3] the first advantages of hBN where reported, reporting a mobility of 140.000 $\text{cm}^2\text{V}^{-1}\text{s}^{-1}$. Theoretical calculations have been performed in [27] relating the experimental data in [3] to impurity concentrations. A distinction is made between long-range disorder characterized by randomly distributed charged impurity centers with a 2D intensity of n_i located at the graphene hBN-interface, and the short-range disorder characterized by an effective strength of $n_d V_0^2$ denoting a white-noise delta-correlated local disorder (i.e. formed by adatoms and vacancies). The long-range disorder will typically increase intervalley scattering (within a Dirac cone K or K'), and short-range disorder will often induce intravalley scattering (scattering form cone K to K' or vice versa). Their calculations reveal that the charged impurity density n_i has the remarkably small value of $0.3 \cdot 10^{11} - 1.0 \cdot 10^{11}\text{cm}^{-2}$ for graphene on hBN substrates compared with $n_i > 10^{12}$ cm^{-2} for graphene on SiO_2 substrates. The short-range disorder seemed comparable in strength for hBN and SiO_2 substrates.

In this project a hBN thickness of approximately 30-40 nm has been chosen; this width is thick enough to compensate for the underlying SiO_2 roughness, and it is still possible for electrodes to overcome the step in height from SiO_2 (which still forms the backgate) to hBN.

2.4 Raman spectroscopy measurements

Section 3.1.1 will describe how graphene flakes can be found with an optical microscope. Using contrast values one can actually distinguish between mono-, bi- and trilayers. These contrast values however do not always give absolute certainty about the amount of layers; therefore Raman spectroscopy has been performed on each flake to be certain. This section will describe the basic principle of Raman spectroscopy and show a Raman spectrum for a mono-, bi- and trilayer.

Raman scattering is the inelastic scattering of a photon. The photon excites an electron from the ground state g_0 to a virtual state that can subsequently relax to a lower vibrational state g_1, and emits a second photon. The scattered photon has a slightly lower energy than the incident

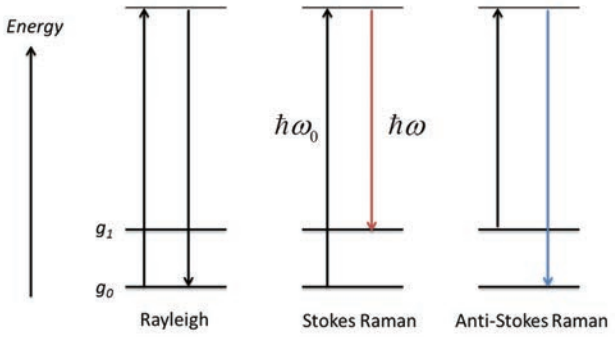

Figure 2.5: Schematic overview of Raman scattering. An incident photon with energy $\hbar\omega_0$ can excite an electron to a virtual state. Most of the time the electron relaxes back to the ground state: Rayleigh scattering. A small fraction makes the transition to the nearby vibrational state: Raman scattering. If the molecule absorbs energy it is called Stokes scattering, when the molecule loses energy it is called Anti-Stokes scattering.

photon. This energy difference corresponds to the energy of a certain vibrational mode of the system. This process is shown schematically in Fig. 2.5. The Renishaw setup can detect the energy difference $\hbar(\omega_0 - \omega)$ which is called the Raman shift.

Spectra taken from [30] have been used to distinguish between the number of layers; see Fig. 2.6 for an overview. The major differences between the spectra are found in the typical shoulder around 2660 cm^{-1} (2D-peak) for a bilayer, and the slope of the 'horizontal' part of the peak (it's positive for a bilayer and negative for a trilayer). For the discussion in chapter 4 it is also useful to know that graphene with defects has a D-peak at 1350cm^{-1}; this allows us to see whether our processing influences the quality of our graphene. The D-mode originates from the 'breathing' of a sixfold ring and this mode is not allowed for defect-free graphene since two neighbouring rings cannot expand and compress at the same time.

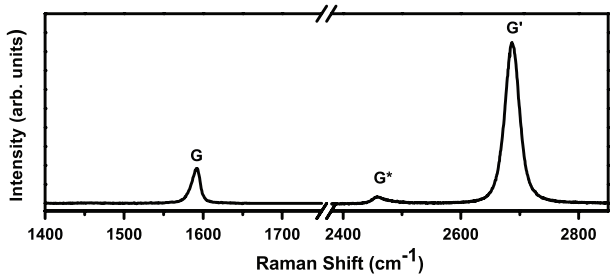

(a)

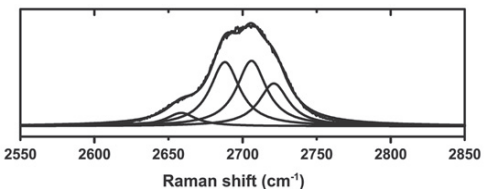

(b)

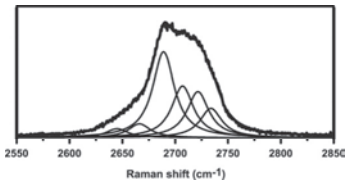

(c)

Figure 2.6: Raman spectra taken from [30] for a (a) monolayer, (b) bilayer and (c) trilayer.

2.5 Experimental realisation

This section will be a mix between theory and actual practice. Here we will give estimations for the expected charging energy E_C and level spacing E_s in our dot, and also describe the measurements that ought to be performed to start using the dot.

2.5.1 Estimation of the charging energy and level spacing

To calculate the charging energy under the assumptions described in section 2.2 we only need the total capacitance of the dot system, i.e. $C = C_S + C_D + C_{BG} + C_{TG} + C_{PG} + C_{\text{self capacitance}}$. To make a first estimation for the upper bound of E_C, C_{BG} and $C_{\text{self capacitance}}$ will be calculated. This value will then be compared with a typical E_C from a similar GaAs dot.

C_{BG} is modelled as a parallel-plate capacitor made of a layer of 285 nm SiO_2 and 40 nm hBN, both have a relative dielectric constant ϵ_r of approximately 4 [3]. This allows us to model the two layers as one 325 nm thick layer of dielectric with $\epsilon_r \approx 4$. Estimating the area A of the dot as a circle with diameter $D = 100$ nm (see section 3.7) we find:

$$C_{BG} = \frac{\epsilon_r \epsilon_0 A}{d} = 0.9 \text{ aF} \tag{2.5}$$

where $\epsilon_0 = 8.85 \cdot 10^{-12}$ F/m. The self-capacitance of a circular disk is given by $4\epsilon_r\epsilon_0 D$ [31]. The use of this formula is allowed if D is smaller than the length scale of the surrounding dielectric (with $\epsilon = \epsilon_r\epsilon_0$). For our dot $D \approx 100$ nm and the thickness of the dielectric below is ≈ 325 nm and on top ≈ 30 nm. Therefore, the condition is not satisfied on top, which we'll correct for by estimating the 'effective' ϵ as 20% of hBN and 80% vacuum. This gives a self-capacitance of:

$$4(4 + 0.2 \cdot 4 + 0.8 \cdot 1)\epsilon_0 D \approx 20 \text{ aF} \tag{2.6}$$

The upper bound for E_C then becomes: $\frac{e^2}{C} \approx 8$ meV. The true value will be lower due to the capacitances of the source, drain and top- and plungergate. A GaAs dot with $D \approx 200$ nm and an almost similar gate structure has a E_C of 2.4 meV [32]. As the diameter of this dot is twice as large, and $\epsilon_r \approx 12$ of GaAs is 3 times higher, its E_C is expected to be six times smaller, which is approximately the case.

To calculate the level spacing we use the formula from [1]:

$$E_s = \frac{\hbar^2 \pi}{m^* L^2} \approx 0.7\text{meV} \tag{2.7}$$

for L=100 nm and an effective mass of $m^* \approx 0.033 m_e$ [33]. The values for E_C and E_s are both within a measurable range.

A final note can be made about the ratio of the expected voltages needed for the top- and backgates. As the dielectric underneath the topgates is about ten times thinner than that for the backgate, one needs to apply an approximately 10 times lower voltage on the top gates in comparison to the backgate to reach the same amount of doping.

2.5.2 What measurements to perform

When the first device has been made the following measurements are to be performed:

1. Check if the gates are not connected to each other and test for gate leakage.
2. Find the Dirac point by measuring the resistivity versus backgate voltage. A peak in resistivity will occur when the Fermi level crosses the Dirac point. In the ideal case this should

occur for a backgate voltage of 0 V, but in practice the graphene will have some intrinsic doping which will offset the backgate voltage. The height and width of the resistivity peak gives us information on the quality of the graphene flake (the sharper and higher the peak, the better). Also, the offset of the backgate voltage should fall within the limitations of our measurement setup. From this measurement the mobility μ can be determined using the relation $\sigma = ne\mu$ (σ is the conductivity). The value of the doping n can be estimated from the capacitance just calculated. The value of the mobility will help us determine whether the hBN substrate has improved the electronic properties of the graphene. Note: the mobility can be determined in a more precise way by measuring the quantum hall effect; for now we will not need that precision for our experiments.

3. If the first two measurements are good enough it is time to start tuning the dot to the right top- and backgate voltages, i.e. $R_{dot} \gg \frac{h}{e^2}$, and start measuring Coulomb blockade. From the shape of the diamonds information such as the charging energy of the dot can be extracted.

Chapter 3

The dry-transfer method

To be able to create devices as described in the introduction (see for example Fig. 1.1), it is necessary to perform the seven steps as depicted in the schematic overview of Fig. 3.1. This chapter will cover the main idea and motivation for each step and explain what progress has been made during this project in order to optimize the process. Details can be found in the Appendix. It should be noted that other ways have been described as well to transfer graphene involving a wet intermediate step, i.e. with the usage of water [34]. The advantage of that method is that it is relatively easy to position the graphene on top of the target (easy alignment). The disadvantage is the contact with water molecules: these will be trapped in between the graphene and target and thereby influence the electronic properties. These properties are vital for a good QD, and thus a dry-transfer method has been applied which involves no water.

3.1 Finding graphene and hBN flakes

3.1.1 Graphene flakes

On the basis of contrast values as described in [35] and calculations using a Fresnel solver for multilayer films [36] the following substrate for transferring the graphene from tape (standard mechanical exfoliation using Kish graphite [2]) has been designed (see Appendix 8.1.1 for the exact recipe): a Si-wafer with a top layer of ± 50 nm Aquasave[1] and ± 390 nm polymethylmethacrylaat

[1]Produced by Mitsubishi Rayon Co., Ltd

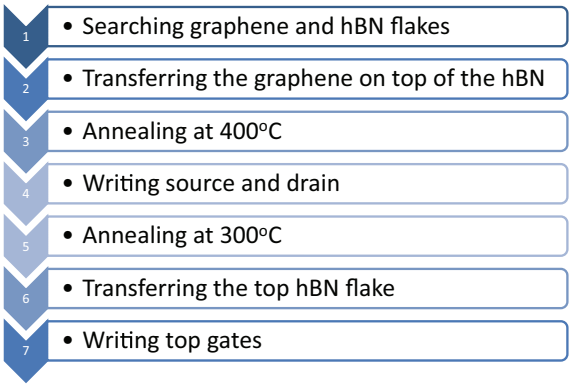

Figure 3.1: Schematic overview of the steps used during the dry transfer method to make a device such as shown in Fig. 1.1.

(PMMA A6 950k), see Fig. 3.2. This combination gives good contrast values of graphene for green light (550 nm), see Fig. 3.3, and allows us to separate the PMMA film (holding the graphene) from the Si-wafer (as described in the following paragraphs).

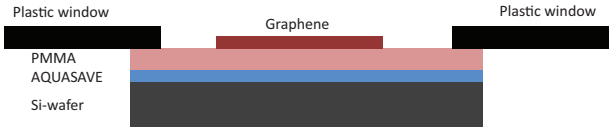

Figure 3.2: Schematic overview of chip used for searching graphene. PMMA-thickness: ±390 nm, Aquasave-thickness: ±50 nm.

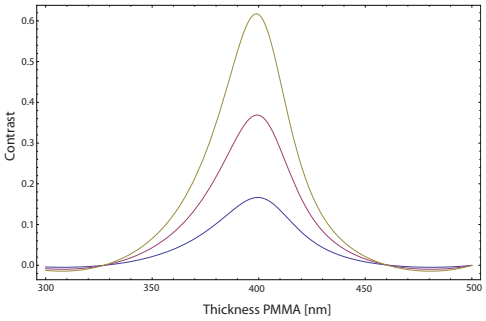

(a)

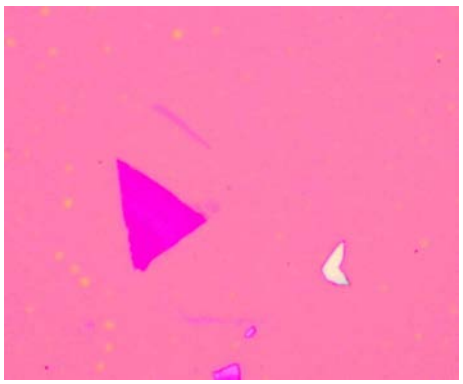

(b)

Figure 3.3: (a) Contrast of unpolarized green light (550 nm) for single layer (blue), bilayer (purple) and trilayer (brown) graphite. This calculation was performed using the following values of the refractive indices: $n_{SiO_2} = 1.46$, $n_{Aquasave} = 1.58 + 1.83i$, $n_{PMMA} = 1.59$ and $n_{graphene} = 2.7 + 1.4i$. The contrast is defined as $I(\text{background})/I(\text{graphene}) - 1$. [35, 36] (b) A bilayer of graphene under the optical microscope (size of the flake: 1.4 x 12 μm).

After the 'optical search' the bilayer-thickness is confirmed by Raman spectroscopy (Renishaw setup with an Ar laser (514.5 nm) using a 50x objective), see Fig. 3.4. The Raman spectra show a large amount of background signal which most likely originates from the layer of Aquasave. Aquasave is a conducting material and will therefore absorb light from the laser; apparently the Aquasave has vibration modes over a large continuous spectrum. This background signal was absent in chips with just a layer of PMMA (and no Aquasave). Despite this large signal we could still distinguish between the amount of layers using [37].

3.1.2 hBN flakes

For the hBN flakes that need to be stamped on top of the graphene, the same procedure as for graphene flakes is applied. The only difference is the colour of the flakes to look for: it has been deduced from AFM images that a thickness of 30-40 nm corresponds to light blue flakes of hBN, see Fig. 3.5. The hBN-flakes used in this study were exfoliated from hBN single crystals that were grown by the method described in ref. [38].

Flakes of thickness ≈40 nm are used for the bottom hBN flakes, and ≈30 nm for the top hBN flakes. 40 nm is thick enough to compensate for the SiO_2 roughness, and thin enough to

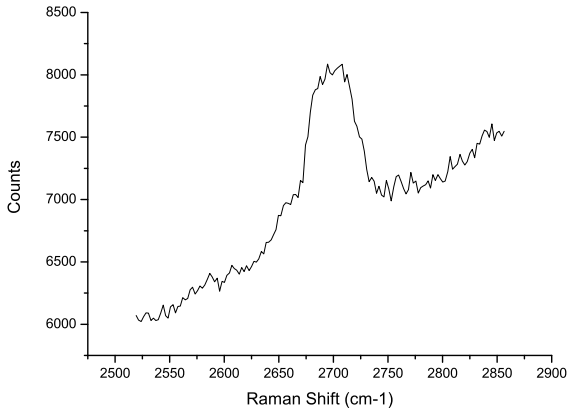

Figure 3.4: Raman spectrum of the graphene flake from Fig. 3.3 with the typical shoulder at $\approx$ 2660 cm^{-1} (2D-peak) [37]. The large background signal is accounted for by the layer of Aquasave.

Figure 3.5: A suitable hBN flake on a chip covered with PMMA.

allow good backgate functionality. The top flake is 10 nm thinner, to ensure that it will be able follow the surface from the source/drain to the graphene well. After finding suitable flakes AFM images of the hBN should be made to check for surface roughnesses and possible contaminations. Approximately 1 out of 10 flakes have the correct thickness, appear clean and flat under the AFM. See Fig. 3.6 and 3.7 for a comparison of a dirty versus clean flake. The relatively low chance of having a flat and clean flake could possibly be explained by the fact that the hBN-crystals will most likely break at the weak spots in the crystal during mechanical exfoliation. These weak spots could be made out of misaligned crystal planes or places where dirt is located inside the crystal. It is however unlikely that pieces of dirt as large as 2 nm are inside the crystal, so those probably originate from elsewhere (it is not yet known where from).

For the bottom hBN layer of the device, the procedure is much easier: now nothing needs to be transferred and the chip is made from a Si-wafer covered with a 285 nm layer of SiO_2 (so that the Si-wafer can function as a back gate) [2]. hBN is deposited on this chip using mechanical exfoliation and the light blue flakes are suitable candidates for the bottom layer of the devices. These flakes have also been AFM'ed to check for surface roughness.

[2]The value of 285 nm is an optimal value to look for graphene if one would use graphene-devices on SiO_2; this is not the case for us so we actually only need a thick enough insulating layer for the backgate-functionality. For practical reasons we already had wafers of 285 nm, so we used those.

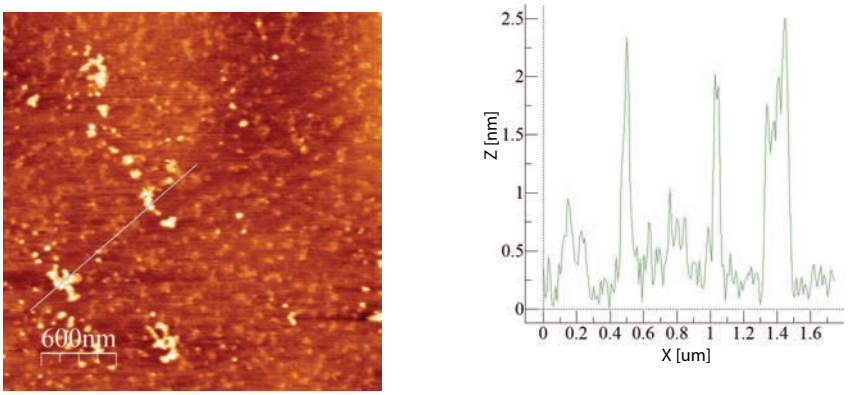

(a) (b)

Figure 3.6: (a) Example of a dirty piece of hBN. (b) Height profile of the blue line in (a).

At the end of the project the observation was made that annealing the hBN flakes on the Si-wafer at 400°C (see 3.3 for details) made all light blue flakes suitable according to the AFM. Unfortunately this annealing cannot be performed on hBN flakes that are on top of the PMMA-Aquasave chips, as the high temperatures changed the composition of the PMMA-Aquasave layer (probably more solvents evaporate). It seems plausible that annealing will remove most of the dirt from the hBN flakes; so it should certainly be tried once more for the bottom hBN flakes to check if it always works.

3.2 Transferring the graphene on top of the hBN

When suitable flakes have been found they need to be sandwiched on top of each other. The first step involves putting the graphene flake on a hBN-chip, this process will from now on be called 'stamping'. To transfer the flake the Si-wafer needs to be removed so that a layer of PMMA + graphene remains. This PMMA (carrying the graphene) will then be suspended in a plastic window which has been attached to the chip; see Fig. 3.8 for an example of hBN on PMMA. The working principle behind this step is the fact that Aquasave dissolves well in water and should thereby release the contact between the PMMA and the Si-wafer.

The alignment of the stamping is done using a small microscope glass with a metallic sphere in it which is open on two sides, see Fig. 3.9 for a schematic overview. First the microscope glass is aligned under the optical microscope with the PMMA-film containing the graphene. The plastic window is covered with two-sided tape and when the alignment is correct the microscope glass and plastic window are brought together so that they stay in contact. Next the hBN-chip is heated to 350°C to remove any dirt and water. After cooling down again, the PMMA-film with graphene is aligned with respect to the hBN[3] and the microscope glass + plastic window are brought into contact with the hBN-chip. During this contact process the hBN-chip is heated to 70°C. It is known from personal communication with the Kim-group (Columbia university) that this temperature should give the least amount of bubbles on the graphene (see chapter 4 for more information on these bubbles, and section 6.2 for a recommendation regarding this temperature

[3]Please note that we are not aiming at aligning the crystal orientation of the graphene and the hBN flakes. Their relative orientation is just a matter of chance in our case. If the two would be aligned though, this will actually create a bandgap as half the carbon atoms see boron B and the other half sees nitrogen N which leads to an asymmetry in potential.

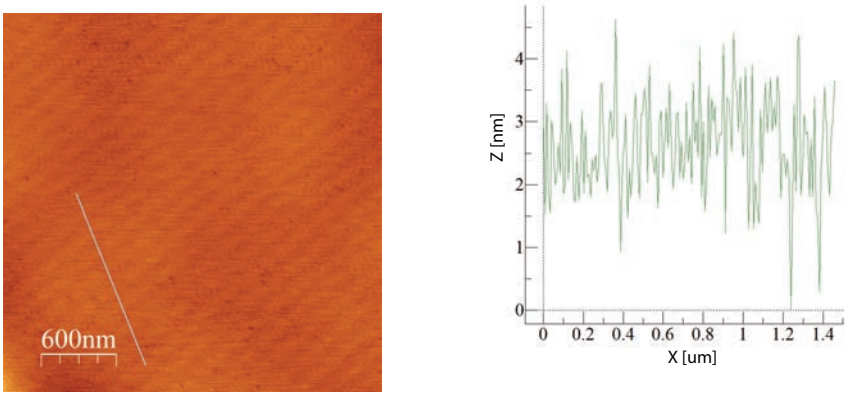

(a) (b)

Figure 3.7: (a) Example of a clean piece of hBN (150 pm surface roughness). The diagonal lines are very likely an artefact in the settings of the AFM which can be removed by further tuning the settings of the feedback loop for the AFM-tip. (b) Height profile of the blue line in (a).

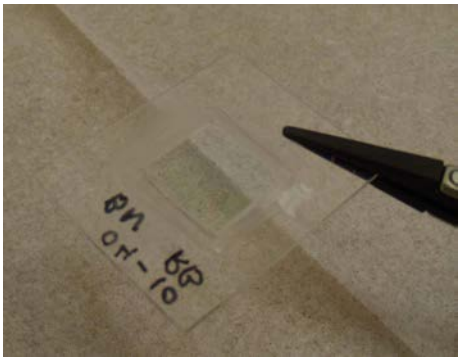

Figure 3.8: Picture of hBN on PMMA suspended in the plastic window after removing the Si-wafer.

(with hindsight it was probably not the best choice)). Next the sample is allowed to cool down and the PMMA is removed with acetone and ethane dichloride. See Fig. 3.10 for an overview.

Other methods used during this project that did not work so well
In the beginning of the project two other ways have been used to release the PMMA from the Si-wafer. They will now be described and explained what there disadvantages are:

Method (1): There was no layer at all between the PMMA and the Si-wafer but just a native layer of SiO_2 (approx. 1.6 nm). This could be dissolved by not putting the plastic window + chip in water, but in a 1M solution of NaOH. This process had several disadvantages; (a) it could take up to 36 hours for the Si-wafer to release itself, (b) the gas formed due to the reaction of NaOH with the Si-wafer would collect underneath the PMMA and lead to severe strain which sometimes ruptured the PMMA-layer, and more importantly, (c) it turned out that the NaOH molecules were able to penetrate through the PMMA and form white crystals on the graphene-side of the PMMA. This would mean that NaOH could contaminate the devices.

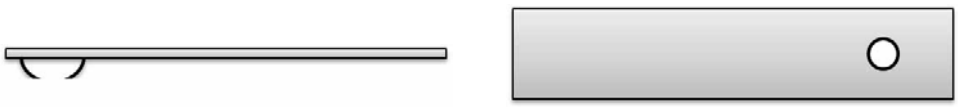

(a) (b)

Figure 3.9: Schematic overview of the microscope glass used for the dry-transfer method (not to scale); (a) side view, (b) top view.

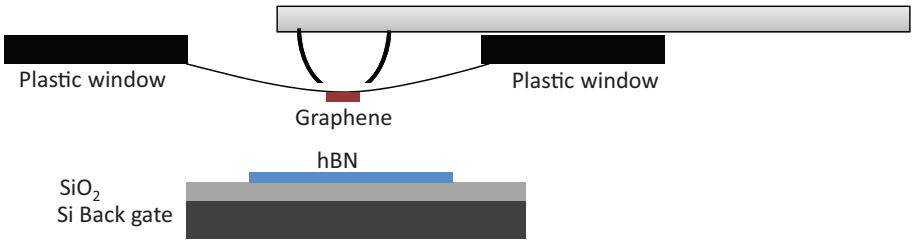

Figure 3.10: Dry-transfer method: first the microscope glass is aligned under the optical microscope with the PMMA-film. The plastic window is covered with two-sided tape and when the alignment is correct the microscope glass and plastic window are brought together so that they stay in contact. This is then aligned with the hBN and the microscope glass + plastic window are brought into contact with the hBN-chip.

Method (2): The layer of Aquasave was replaced by a layer of 10-30 nm polyvinylalcohol (PVA). PVA is also water soluble but it turned out that it did not dissolve quick and good enough for practical purposes. We only once succeeded in successfully dissolving the full PVA-layer.

It must be mentioned that although the method involving Aquasave has a lot of advantages, it has the disadvantage of absorbing quite some light (due to its absent bandgap). Small thickness variations can therefore lead to different reflected light intensities which turned out to actually influence the value of the contrast (and thereby our test for whether a layer is a bilayer or not). In principle one would not directly expect that the value of the contrast changes if the absolute light intensities change (as the contrast is defined as a ratio: $I(\text{background})/I(\text{graphene})-1$). But the light paths describing $I(\text{graphene})$ travel relatively less through the Aquasave than the paths describing $I(\text{background})$, thereby leading to a different response to varying Aquasave thicknesses. Another parameter influencing the value of the contrast is the shutter time of the photocamera which therefore needs to be kept constant.

3.3 Annealing at 400°C

To remove the last pieces of PMMA, other contaminations and 'flatten' the graphene the samples were annealed at 400°C in an argon/hydrogen environment for 2.5 hours. The reasons for this specific temperature are further explained in chapter 4.

3.4 Fabricating contacts (source and drain)

The source and drain are written using standard electron beam lithography[4] to form a 10 nm layer chromium covered by 90 nm of gold. In the beginning of the project titanium was used instead of

[4]These contacts were written and designed by A.M. Goossens.

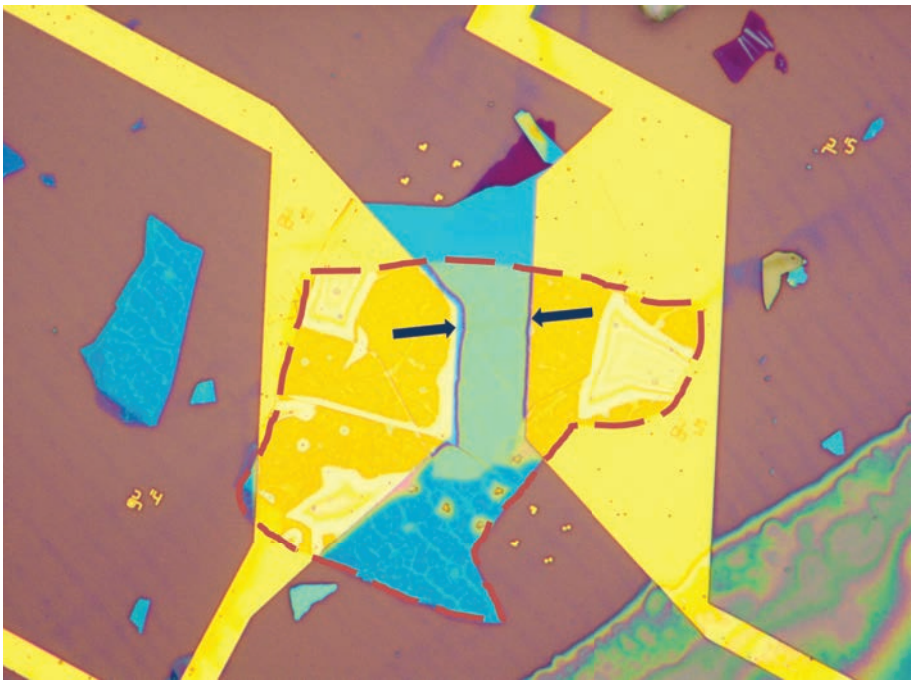

Figure 3.11: Optical-microscope image of the device after step 6 of the dry-transfer method. The red dotted lines indicate the boundaries of the hBN flake that has been transferred as the top layer; it is the same flake as depicted in Fig. 3.5. If one looks carefully you can see the piece of graphene from Fig. 3.3 (b) in between the blue arrows.

chromium, but this did not stick well to the hBN.

3.5 Annealing at 300°C

The sample is annealed once more for the same reason as described in section 3.3. The only difference is that the temperatures is lowered to 300°C to prevent melting of the metallic contacts.

3.6 Transferring the hBN flake

This is almost the same procedure as in step 2 (section 3.2). The only differences are that (1) the chip is not heated to 350°C before the transfer as this would burn the graphene and (2) the transfer itself is performed at 175°C. Especially point (2) took quite some time to optimize. At the start of these transfers they were also performed at 70°C, but these transfer always got misaligned (see Appendix 8.1.4 for an example). It turns out that at 70°C the PMMA film and the hBN do not yet stick to the substrate good enough. If one then applies acetone to remove the PMMA, the hBN-flake will first whirl around randomly and end up somewhere else. At 175°C this problem is solved and the PMMA + hBN stick really well and the alignment is perfect, see Fig. 3.11 for an example.

To check if the top hBN-flake adjusts well enough to the surface profile it covers, an AFM image has been made. Within 1 μm of the source/drain the hBN flake has adjusted completely from the height difference between the graphene and the contacts, and is flat.

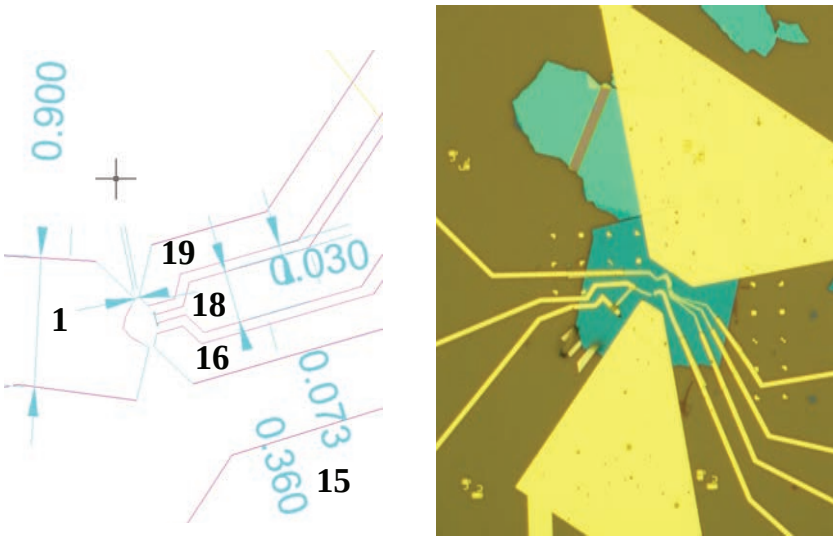

(a) (b)

Figure 3.12: (a) Schematic drawing of the topgatestructure. Blue arrows depict the sizes of the gates, and distances between them. Width of the left split gate: 0.9 μm, size of the constriction: 30 nm, distance in between the three topgates on the right: 73 nm. The numbers on the gates refer to the gates used during the measurements described in section 5.2. Topgate 15 belongs to a non-functional dot (see (b)), but can still influence the doping of the graphene flake at its position. (b) Picture of a completed device (scenario (2)) with two QD-structures. The bottom topgate-structure broke during the lift off procedure and this dot has therefore not been used.

3.7 Fabricating the top gates

The topgates were also written using standard electron beam lithography. Fig. 3.12 shows the shape and sizes of the topgates. During the first trial of writing the topgates, the top hBN-flake was flushed away during the lift off procedure. Therefore we decided to continue with two different scenario's: (1) redo the steps from the previous section to cover the graphene flake again with hBN, and next clamp the top hBN-flake by covering it with PMMA and overexposing it at the sides of the flake. The overexposed PMMA should crosslink and will not dissolve in acetone. The result is shown in Fig. 3.13. (2) continue without covering the graphene with hBN, but instead use SiO_2 as dielectric underneath the topgates. In principle scenario (1) should be better, but it is more time-consuming. It is expected that the SiO_2 from scenario (2) will not influence the dot too much, as it does not cover the graphene area inside the dot.

For scenario (1) the following thicknesses for the topgates were used: a layer of 9 nm chromium and 30 nm gold. For scenario (2): 50 nm SiO_2 covered by 9 nm chromium and 32 nm gold.

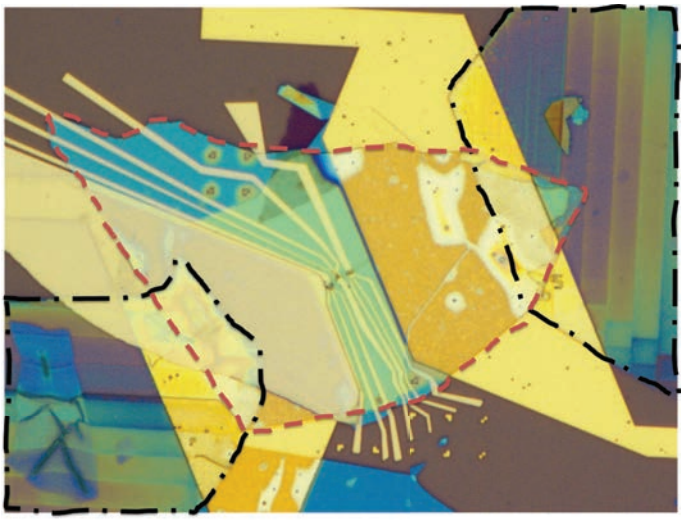

Figure 3.13: An almost finished device from scenario (1). The blue flake within the red circled area is the top hBN-flake. The two black circled areas contain crosslinked PMMA that keeps the top hBN-flake at its position. There is still some gold on the left contact which did not yet lift off properly.

Chapter 4

Annealing of graphene on hBN

When the graphene flakes have been transferred on top of the hBN AFM-images were made to check the positioning of the flakes and the surface-roughness of the graphene. These images revealed that large bubbles were formed on top of the graphene, sizes varying from 5 nm high, 100 nm wide to 40 nm high and 500 nm wide; see for example Fig. 4.1. These bubbles/surface ripples will lead to local changes in the bandstructure which will make the electron properties non-uniform over the device. Therefore it has been tried to remove the bubbles by annealing the graphene on hBN in an annealing oven for 2.5 hours with an environment of argon and hydrogen gas (Ar: 2.4 L/min, H_2: 0.7 L/min). The results of this experiment were used to determine the best annealing temperature to achieve the most flat pieces of graphene whilst not creating any defects (determined by Raman) and have been applied in step 3 and 5 of the dry-transfer method. Also, during the experiments, a relatively large bubble of 500 nm high was formed and we tried to deduce what filled the space underneath the bubble.

4.1 Finding the optimal annealing temperature

The temperatures have been varied from 200 to 800°C in steps of 200°C. After each temperature step AFM-images were made to characterize the 'bubble behaviour'. An overview is shown in figures 4.1 till 4.10. All these figures have been made from the same sample and as an exception to the procedure described in section 3.2 this sample had not been heated to 70°C during the transfer; this enabled us to see the starting condition of graphene without any annealing.

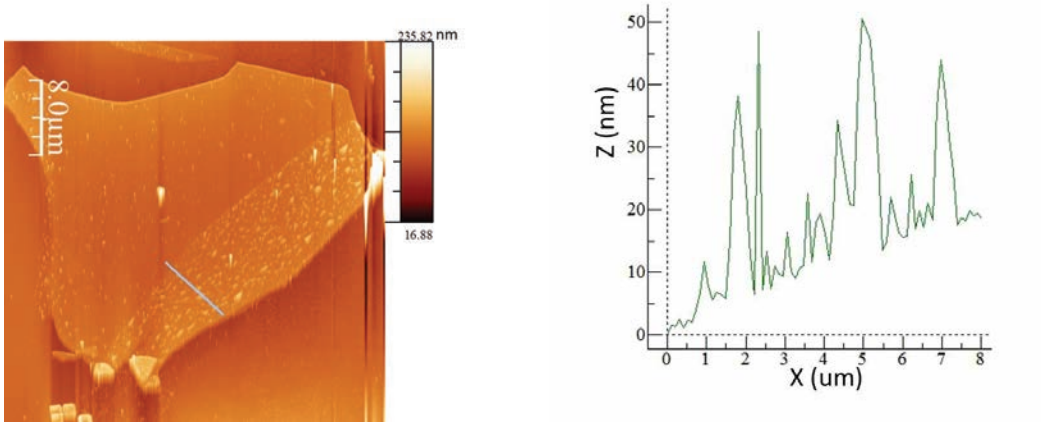

(a) (b)

Figure 4.1: (a) AFM image of a graphene flake on hBN; the hBN-flake is the large structure, the graphene-flake is the part where all the bubbles are (this is known from comparison with optical images). The graphene contains lots of bubbles that are approximately 40 nm high and 500 nm wide. (b) Height diagram of the blue line drawn in (a).

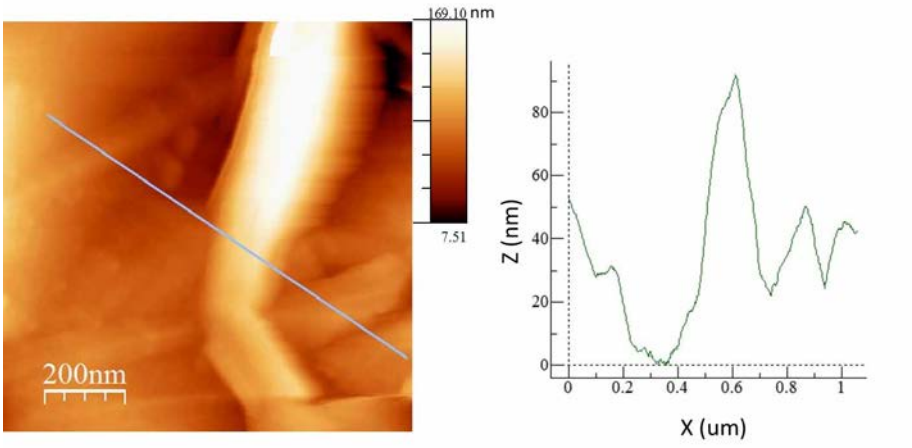

Figure 4.2: Zoom in of Fig. 4.1 on a piece of graphene.

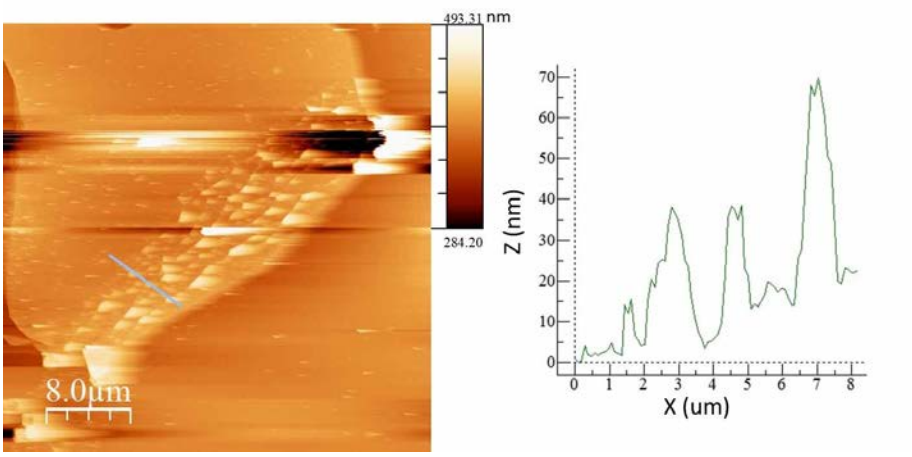

Figure 4.3: Annealing at 200 °C.

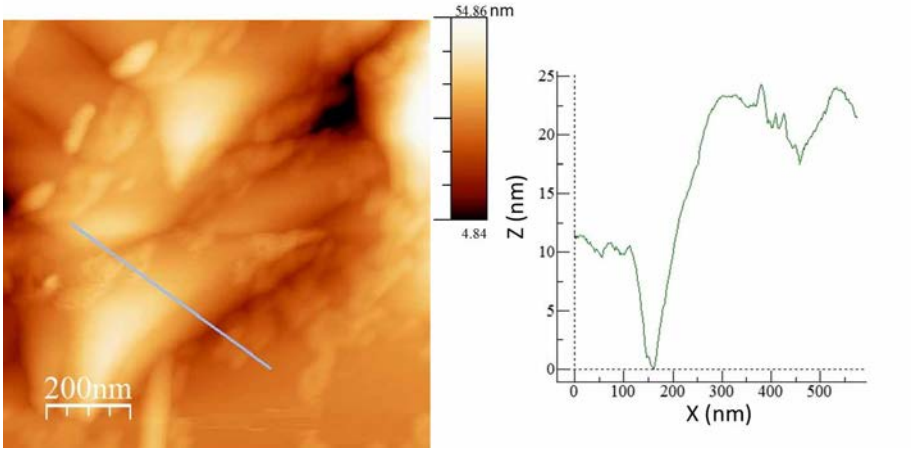

Figure 4.4: Zoom in of Fig. 4.3 on a piece of graphene in between the bubbles.

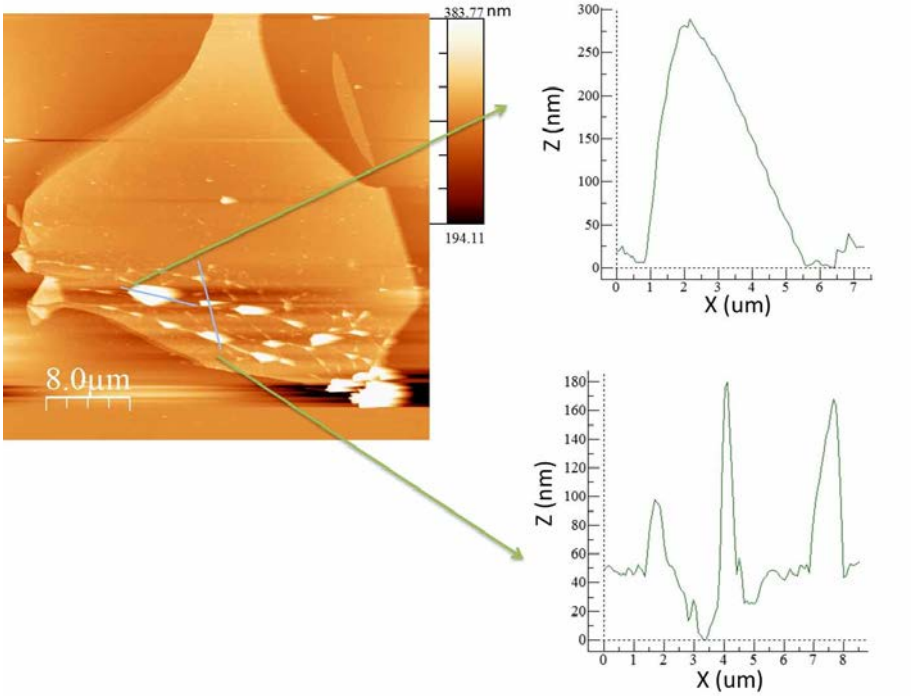

Figure 4.5: Annealing at 400°C.

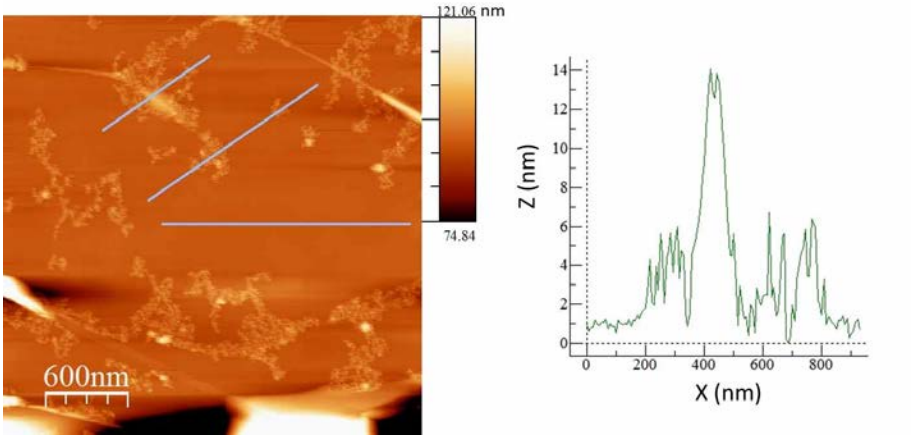

Figure 4.6: Zoom in of Fig. 4.5 on a piece of graphene in between bubbles. Height profile corresponds to the top blue line.

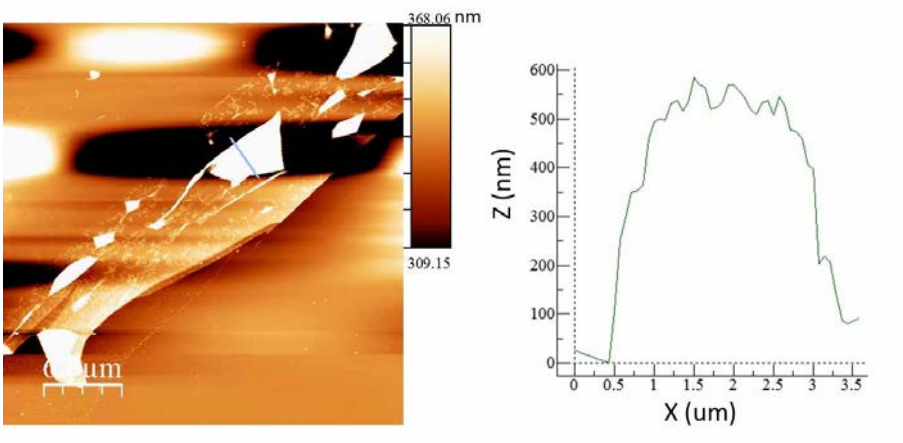

Figure 4.7: Annealing at 600°C.

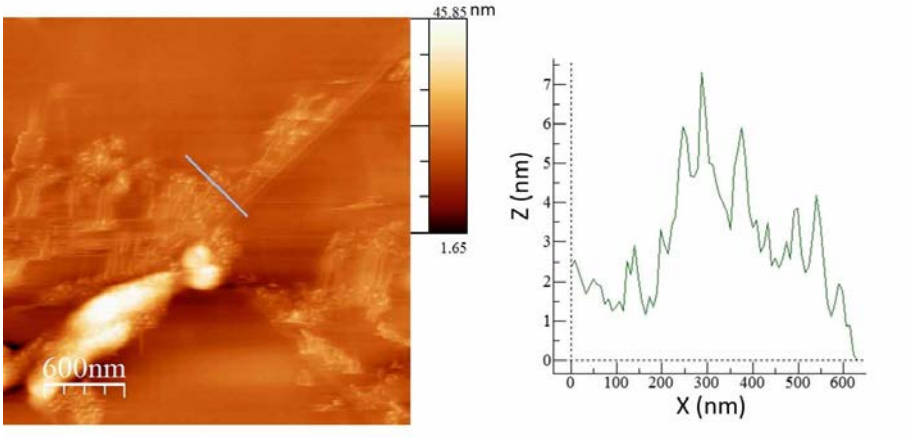

Figure 4.8: Zoom in of Fig. 4.7 on a piece of graphene in between bubbles.

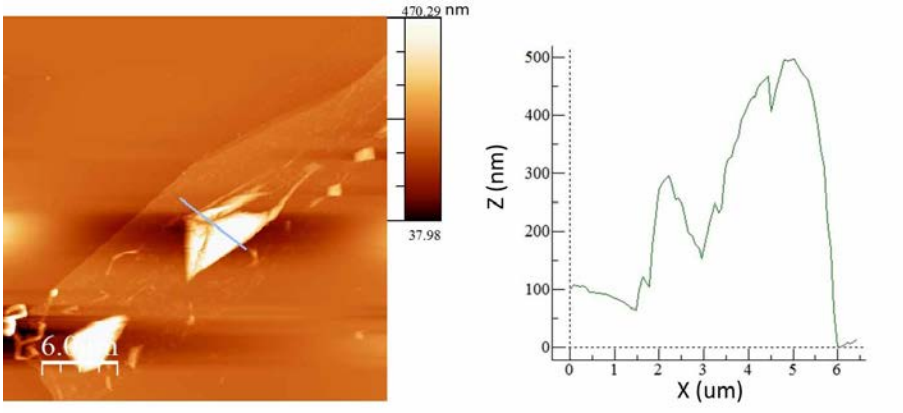

Figure 4.9: Annealing at 800°C.

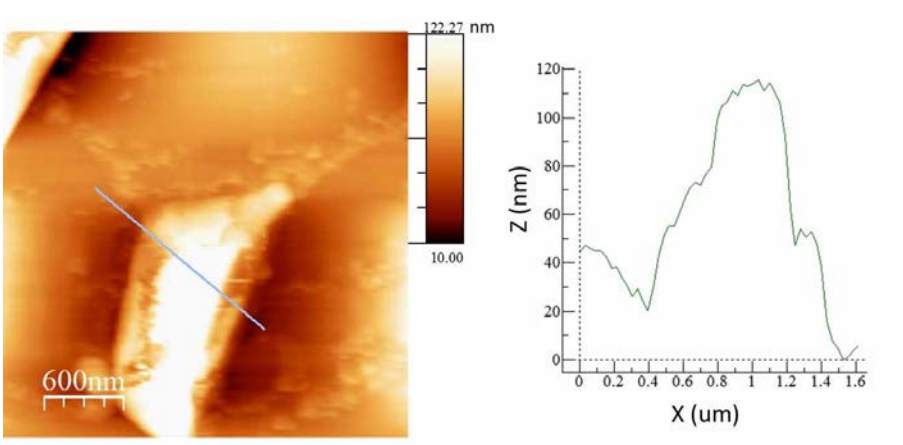

Figure 4.10: Zoom in of Fig. 4.9 on the small bubble right to the big bubble in the bottom left.

From Fig. 4.1 till 4.10 a general trend is observed of smaller bubbles coalescing into bigger bubbles. The formation of larger bubbles has also been seen in three other samples together with the observation that relatively large (around $1\mu m^2$) flat areas arise in between the bubbles. These areas could in principle then be used as material for the QD. The high annealing temperatures might however alter the graphene itself. Therefore a Raman has been performed after the annealing at 800°C which is depicted in Fig. 4.11. The red curve has been measured on the hBN substrate, the black line on the SiO_2. In both cases the characteristic shoulder at $\approx$ 2660 cm^{-1} is not clearly visible anymore and the emergence of a D-peak is seen around 1350 cm^{-1}. This D-peak indicates that there are defects in the lattice due to non-perfect sp^2-hybridization and means that the graphene is not a good bilayer anymore and thus that this annealing temperature is too high for further processing. Another striking feature is the positive slope in the red line, this should not be there (as the hBN should have a too large bandgap (~6 eV)) and indicates that something might be wrong with the hBN as well. This experiment has been repeated in order to find the optimal annealing temperature where no D-peak occurs. The result is that one can go up to an annealing temperature of 400°C without deteriorating the graphene.

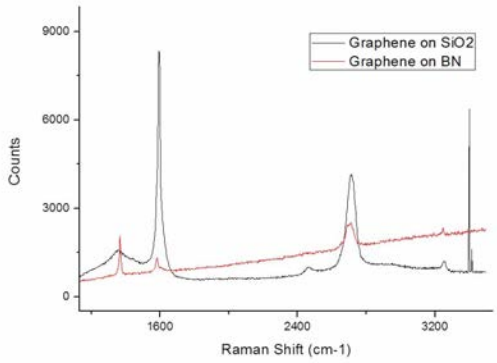

Figure 4.11: Raman spectrum of the graphene flake from Fig. 4.9. The red curve has been measured on the hBN substrate, the black line on the SiO_2. In both cases the characteristic shoulder at $\approx$ 2660 cm^{-1} is not clearly visible anymore and the emergence of a D-peak is seen around 1350 cm^{-1}.

4.2 Behaviour of bubbles in bilayer graphene

Although we can optimize the flatness of the graphene now, it is still far from perfect. To better understand why the bubbles are there and what's underneath them, we continued with a sample that had been annealed up to 400°C and performed a Raman spectrum line-scan over a large bubble of approximately 250 nm high and 2 μm wide. The results are depicted in Fig. 4.12. This line-scan was also partly motivated by a suggestion given in personal communication with Fal'ko and involves the splitting of the bilayer graphene into two monolayers as shown in Fig. 4.13. A splitting of the layers would lead to a monolayer Raman spectrum at the location of the bubble. This possibility is motivated by the suggestion that the monolayer in contact with the hBN will feel different forces than the top-monolayer. These differences in strain could lead to the splitting.

To correct for the extra base-signal that the hBN gives (see for example the red curve from Fig. 4.11) a baseline has been fitted to all Raman spectra and subtracted from the data. Also, all spectra have been normalized to the value of the silicon peak at approx. 520cm^{-1}. The uncorrected Si-peak varied less than 10% during the measurement and should in principle stay constant.
Fig. 4.12 (b) shows that the graphene stays bilayer on the location of the bubble (i.e. line-scan 8, 9 and 10) which contradicts the suggestion from Fal'ko. This was already expected as the aspect ratio of the bubbles suggests that the top monolayer needs not to be stretched severely to follow the shape of the bubbles. Other interesting features are:

- The ratio of the height of the G-peak (at 1580 cm^{-1}) and the 2D-peak. The G-peak is more prominent at the location of the bubble; this is most likely explained by the fact that the interaction between the substrate and the graphene differs on the bubble in comparison to next to the bubble.
- The height of both the G- and 2D-peak is higher on the bubble. This means that more vibrations have been excited per mode, which seems plausible if one keeps in mind that the graphene atoms should be relatively more free to move if semi-suspended.
- The signal from the hBN and silicon remains nearly constant which implies that no light is absorbed underneath the bubble[1].

It is not yet known with certainty what is precisely happening under the bubbles. The most convincing explanation at this moment is that gas is trapped underneath the graphene when the graphene is lowered onto the hBN-chip. This is supported by the following arguments: (1) From Fig. 4.1 till 4.10 a general trend is observed of smaller bubbles coalescing into bigger bubbles. This is in accordance with the 'general principle' that the pressure in smaller bubbles will be higher than in large bubbles (compare with inflating a balloon, first part requires more pressure) and suggests that gasses are underneath the bubbles. (2) The Raman measurement demonstrates that almost no light is absorbed underneath the bubble, this would most likely not have been the case if some solid had been there. (3) The bubbles decrease in height and tend to spread when stored in vacuum at room temperature for several weeks. (4) Other research groups have shown that gas can be trapped underneath graphene [39]. There is however one counter argument: as a final test we have put the chip containing the bubble in liquid nitrogen for approximately one minute: nothing changed however when it was restored to room temperature. We had expected that the gas in the bubble would contract and expand, which should have led to some changes in shape: this did not happen.

The formation of larger bubbles led to relatively large flat areas in between the bubbles suitable for QD's. However, there still remain typical contaminations such as those shown in Fig. 4.6 on the flat areas. Comparison with other samples shows that there are no such contaminations before the sample has been in the annealing oven. The SEM in Fig. 4.14 shows that the contaminations

[1] If this experiment will be repeated, it is important to check the focus of the laser spot during the line-scan. Due to height variations the focus might change (the focus depth of the used lens is not known).

are also there on or under the surface of a bubble. From this we can conclude that the contaminations in each case attach better to the graphene than to the hBN, but not yet whether they are on top of the graphene flake or in between the hBN and the graphene. It could be that (1) a piece of dirt elsewhere on the substrate starts spreading during annealing, or (2) the oven itself is contaminated. At this moment (1) seems to be the most likely cause, as another type of sample from V.E. Calado did not suffer from these type of contaminations when it had been annealed in the same batch.
Another explanation for some of the small wrinkles and bubbles that can be seen comes from the roughness of the hBN itself. After this annealing-experiment the surfaces of the used hBN-crystals have been AFM'ed and these turn out to be quite rough as well sometimes. From then on, AFM's have always been made to pick the smoothest hBN flakes.

The important things we have learned from these experiments are that (1) the optimal annealing temperature is 400°C which gives rise to flat areas of graphene that can be used for QD's, (2) hBN flakes should be AFM'ed before usage and (3) a bilayer stays a bilayer when it forms a large bubble.

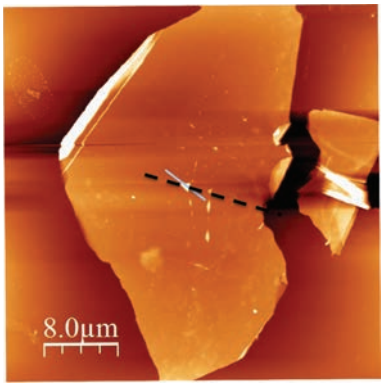

(a)

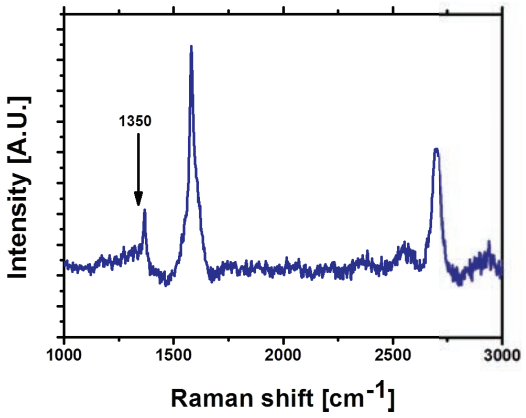

(b)

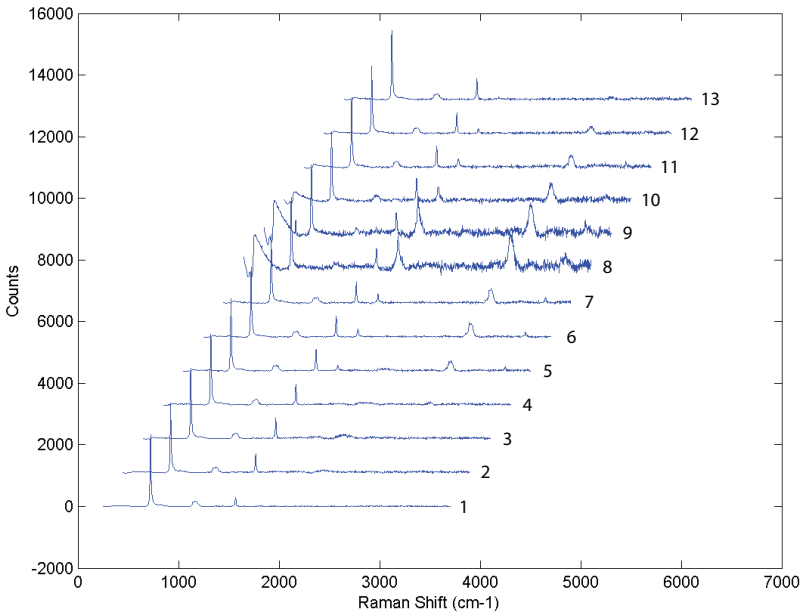

(c)

Figure 4.12: (a) Striped black line: location where the Raman line-scan shown in (b) has been measured (total length: 12 μm in steps of 1 μm, from right to left). (b) Spectrum on the bubble; no (or very small) signal at D-peak position. The typical shoulder of a bilayer at 2660 cm^{-1} is still visible. (c) Raman line-scan spectrum normalized to peak-value of silicon (the peak at approx. 520 cm^{-1}), baseline has been subtracted; see text for details. Counted from below: the first three spectra are on hBN (no graphene), line 8, 9 and 10 are on the bubble.

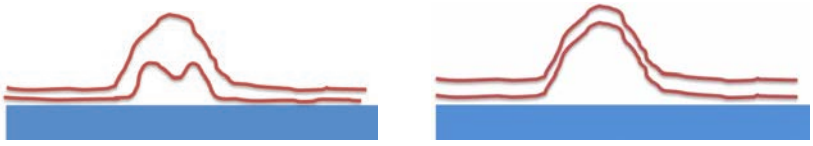

(a) (b)

Figure 4.13: Two possible scenarios for what happens with the graphene bilayer inside a bubble: (a) the bilayer splits into two monolayers due to differences in strain felt by the two layers, (b) the whole bilayer bends into the shape of the bubble.

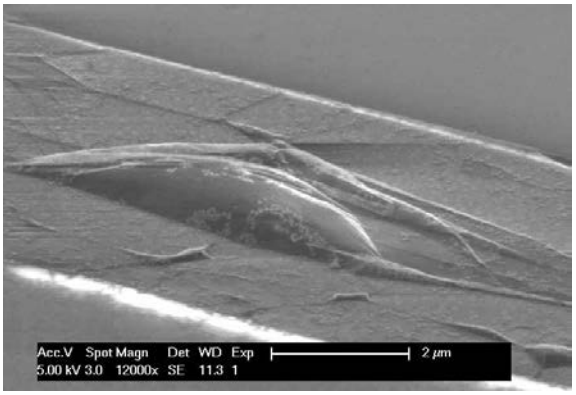

Figure 4.14: SEM of the graphene flake shown in Fig. 4.9 showing the same contaminations on top of the bubble as in e.g. Fig. 4.6.

Chapter 5

Experimental setup and measurements results

5.1 Experimental setup

The measurements are performed in a dilution refrigerator with a base temperature of 50 mK. Each contact on the sample is connected via a copper powder filter at low temperature which filters from 100 MHz to 40 GHz, a two stage RC filter which filters from 10 kHz to 500 MHz at low temperature and a room temperature Pi-filter which filters from 10 MHz to 10 GHz. The filters are needed to prevent an increase of the base temperature due to energy gained from the environment. The DC resistance of each wire is around 2.53 kΩ.

5.2 Measurement results

We have only had time thus far to measure a device from scenario (2), i.e. with SiO_2 as topgate dielectric. This section will present our first measurement results at 4 K and 50 mK. The results at 4 K were not really promising so it has been decided to current anneal in between the two temperatures. At 50 mK the resistance has been measured as a function of the topgates and backgate voltage. These measurements show the first signs of resistance-modulation by the gates.

Tests for gate leakages revealed that the topgates are capable of going from -20 to 20 V without significant leakage. The backgate showed no leakage within -67 to 67 V. A backgate sweep at 4 K for $V_{Bias} = 10$ mV is depicted in Fig. 5.1 (a). A current modulation by a factor of 2 is seen, and apparently the graphene is heavily doped as the charge neutrality point lies at a position $V_{BG} > 67\ V$. A dip in the current is also seen around $V_{BG} = 30$ V and can be explained by assuming that the doping varies over the graphene flake. So some pieces of the flake will cross the Dirac point for different backgate voltages than other pieces.
We have also corrected for the current + voltage offset and resistances of the measurement setup and converted this in a value for the resistance of the sample in Fig. 5.1 (b). The sample resistance is ~ 180 kΩ for zero backgate voltage. This value is really large and will make it difficult to see any topgate induced resistance-modulation at the location of the QD: its relative influence to the total resistance will be low. Sweeps of topgate 1, 16, 18 and 19 (see Fig. 3.12 (a) for the numbering) have been performed from -10 to 10 V for several different voltages at the backgate and topgate 15, but none showed any significant and reproducible resistance-modulation.
Another sign showing the bad quality of our sample comes from an underestimate of its mobility μ. From Fig. 5.1 (a) μ can be calculated using:

$$\mu = \frac{\sigma}{en} = \frac{d}{\epsilon_r \epsilon} \frac{\mathrm{d}\sigma}{\mathrm{d}V_{BG}} = \frac{ld}{b\epsilon_r \epsilon V_{SD}} \frac{\mathrm{d}I}{\mathrm{d}V_{BG}} \approx 6\ \mathrm{cm^2 V^{-1} s^{-1}} \tag{5.1}$$

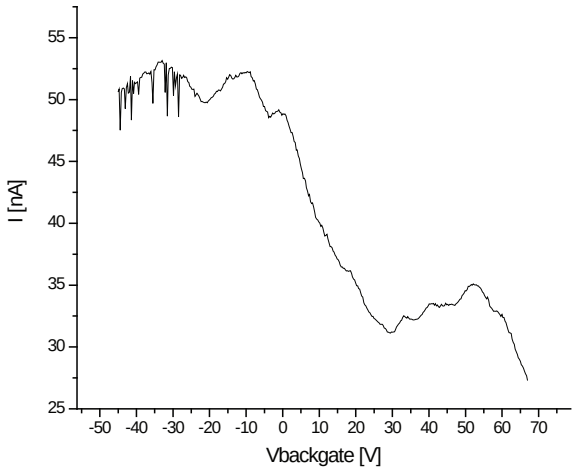

(a)

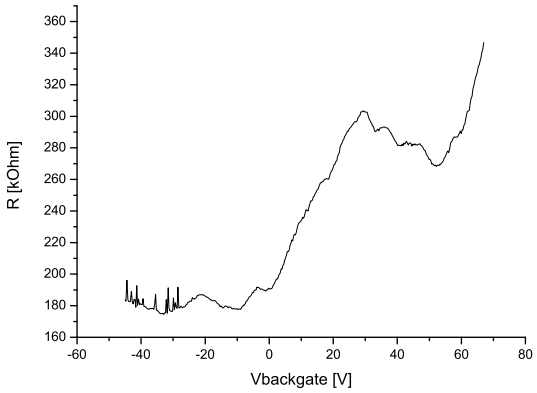

(b)

Figure 5.1: (a) Current as a function of the backgate voltage; $V_{Bias} = 10$ mV, $T = 4$ K. All other gates are grounded. (b) Resistance as a function of the backgate corrected for: voltage and current offset, input resistance measurement setup, and the filter-resistance.

where l is the length of the flake of graphene (≈ 7 μm), b its width (≈ 8.5 μm) and d the thickness of the dielectric (≈ 325 nm). $\frac{\mathrm{d}I}{\mathrm{d}V_{BG}}$ has been measured between 61 and 69 V leading to 0.8 nA/V. This value of the mobility is an underestimate, as the V_{SD} should have been the voltage drop over the graphene flake (and not over the graphene flake + contact resistance). The contact resistance is however unknown. In each case, a $\mu \approx 6$ cm^{2}V^{-1}s^{-1} is orders of magnitude smaller than we had hoped for.

The next step was therefore to current anneal the sample. Current annealing led to a resistance drop of 180 kΩ to 30 kΩ at zero backgate voltages. This makes it more likely to see resistance-modulation by the gates. A new backgate-sweep ($T = 50$ mK, $V_{Bias} = 1$ mV) however did not indicate much improvement, see Fig. 5.2. This spectrum is reproducible, but does not show a clear signature of a Dirac point. The doping might vary so much now over the whole flake, that many small pieces of graphene each reach their Dirac point for different backgate voltages. As a last check to measure the device functionality, a sweep of topgates 1, 16, 18 and 19 versus the backgate and topgate 15 has been performed. Gate 15 belonged to a nearby quantum dot, and to ensure

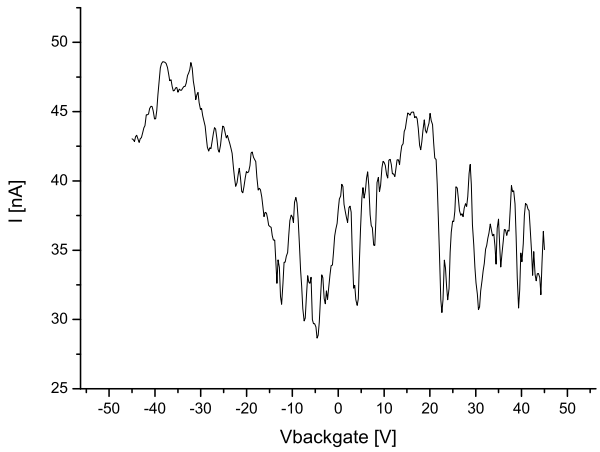

Figure 5.2: Current as a function of the backgate voltage; $V_{Bias} = 1$ mV, $T = 50$ mK. All other gates are grounded.

that we did not block any transport underneath this gate, it was swept along with the backgate. The backgate was swept from -30 to 67 V, and gate 15 from 0 to 20 V at the same time. In this way gate 15 and the backgate tend to induce the same doping. The results are shown in Fig. 5.3. Figure (a) clearly demonstrates that the backgate has the most influence on the resistance, and tends to overrule the influence of the topgates. This could already have been expected by looking at the relatively large current fluctuations from Fig. 5.2 (25%). To still get some insight in the behaviour of the top gates, we normalized the data from Fig. 5.3 (a) in the direction of the backgate taking the peak-value for the resistance as 1. In this way we correct for the large current fluctuations caused by the backgate. From Fig. 5.3 (b) we clearly see that the topgates and the backgate together can reduce the current, and thereby 'push' the Fermi-level to the Dirac-point. We however cannot tell if we have opened a bandgap. Bandgap creation implies that for larger voltage differences between the top- and backgate, the resistance of to the neutrality point should increase. Due to our normalization procedure, we have however lost the information about the absolute height of the resistance and cannot make any conclusions about the bandgap.
From the slope of Fig. 5.3 (b) we can conclude that the topgates are approximately 6 times more effective in inducing charge on the graphene. This agrees very well with what one would expect from the fact that the dielectric underneath the topgates is 6 times thinner than that of the backgate.

Although we see influence of the gates on the graphene-system, the conditions are far from ideal and we have therefore decided to stop measuring this device, and continue with a device from scenario (1). The one being made now (see Fig. 3.13), has a room temperature resistance of 20 kΩ and has less bubbles on its surface which makes it a more promising candidate.

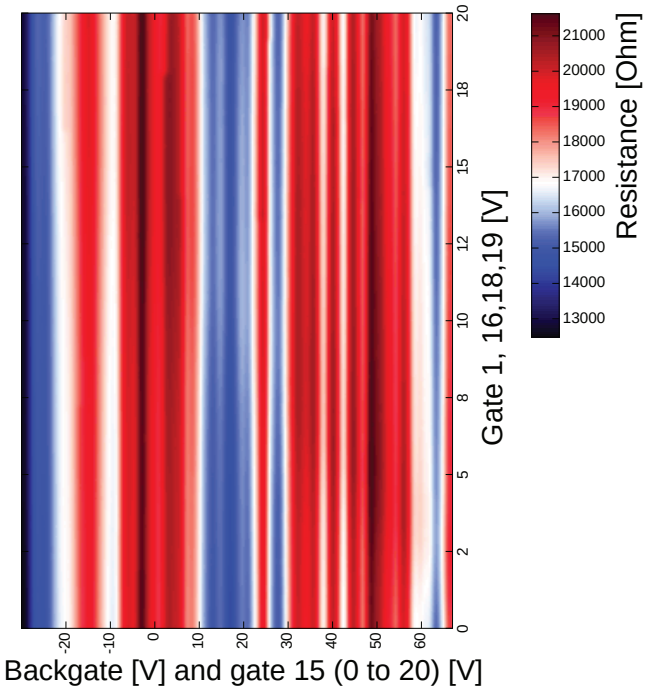

(a)

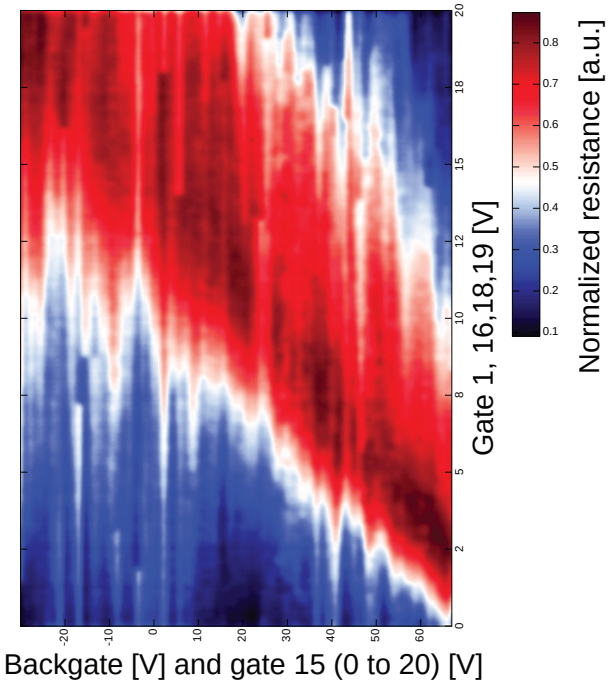

(b)

Figure 5.3: (a) Resistance as a function of the backgate voltage (swept from -30 to 67 V) + topgate 15 (swept from 0 to 20 V simultaneously), and topgates 1, 16, 18 and 19. $V_{Bias} = 400$ μV, $T = 50$ mK. All other gates are grounded. Resistances have been corrected for: current and voltage offset, input resistance measurement setup, and the filter-resistance. A Gaussian smooth has been applied to the data with an averaging of 2 datapoints in x- and y-direction. (b) Same measurement as in (a), but now the data has been normalized in the direction of the backgate and the peak-value for the resistance taken as 1.

Chapter 6

Conclusion and outlook

6.1 Summary of the results

During this project a method has been developed to fabricate the structure for a quantum dot on bilayer graphene made on a boron nitride substrate such as shown in Fig. 6.1. Intermediate steps have been optimized to improve the quality of our devices. The result is a recipe that allows the transfer of graphene using a thin layer of PMMA, on top of a hBN flake without contacting water (i.e. a dry-transfer method). Next, the 'sandwich' is completed with a top hBN flake in the same kind of manner. In between and after these two transfers an annealing step should be performed for which the optimal temperatures (400°C and 300°C respectively) have been investigated. At these specific temperatures the relatively small bubbles (40 nm high and 500 nm wide) of the graphene sheet tend to coalesce and form larger bubbles (200 nm high and 2μm wide), without creating defects in the graphene (confirmed by Raman spectroscopy). The result is a landscape with some large bubbles, with in between flat areas of graphene that can be used as location for the quantum dot. Finally, the type of metal used for fabricating the metallic contacts has been changed from titanium and gold to chromium and gold. The first option does not stick well enough to the hBN, while the second does. The completion of this 'recipe' takes about 1.5 to 2 weeks and the first complete device has just been made. The first measurements will be done in the coming weeks and should reveal whether the usage of the substrate hBN indeed improves the device-quality (i.e. increased mobility) and hopefully Coulomb blockade will be seen. If the results are indeed promising, it is relatively easy to fabricate more devices.

Parallel to the main goal of making a device such as described above, an intermediate kind of device has been completed and measured in the mean time. For that specific device the top hBN-flake has been replaced by silicon oxide at the location of the top gate-structures (so no silicon oxide on the graphene area of the dot). The measurement results show that it is possible to influence the Fermi-level inside the device by the top- and backgates. But the backgate influence on the resistance showed relatively large fluctuations (25%) which did not follow any general trend (such as the shape of a Dirac cone). This made it difficult to deduce the modulation of the resistance if both the top- and backgates were varied. By normalizing the data we were able to show that the gates can bring the Fermi-level to the Dirac point. The topgate turned out to be 6 times more effective in inducing charge, which was in accordance with the predictions. The normalization step however should not be necessary to get these results, and also does not allow us to check for the opening of a bandgap.

At the moment of writing this report, a new device has been made that fully complies with the original goal of this project and uses hBN as a top dielectric. This device contains less bubbles and seems to be more clean which makes it a promising candidate for being the first QD of bilayer graphene made on a substrate of hBN.

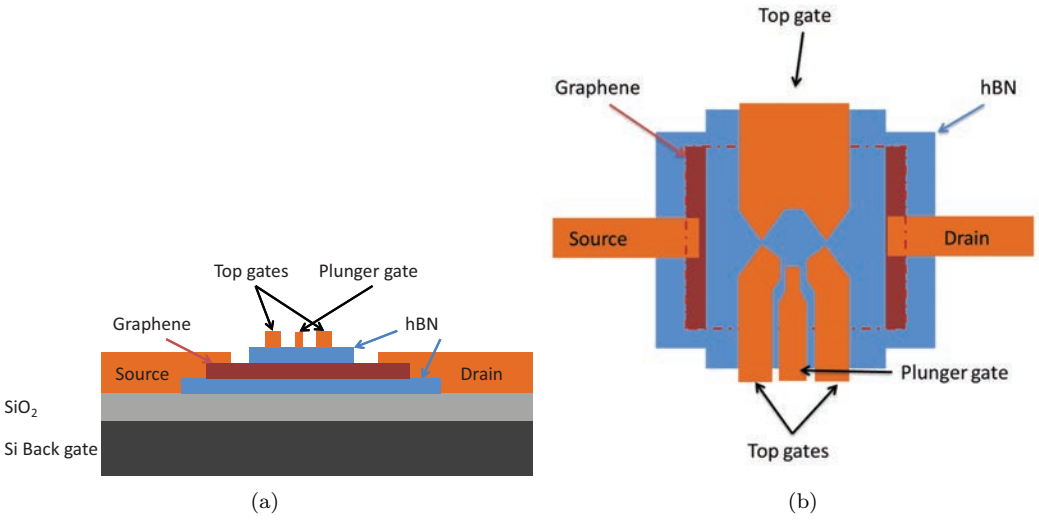

Figure 6.1: Schematics of the device structure (not to scale); (a) side view, (b) top view.

6.2 Future directions/recommendations

Most time of this project has been spend on fabricating devices, and we are now in a phase where we can relatively easy fabricate 2-3 devices within 2 weeks. The first measurements on a similar kind of device however showed poor device functionality. Therefore improvements still need to be made and this section will give recommendations on how to reach those goals. This section will conclude by describing what interesting measurements can be performed in the near and far future.

6.2.1 Recommendations to improve the device quality

At this moment there are two main problems with our devices that most likely decrease the chance of high quality samples:

1. The graphene sheets tend to contain many bubbles. This leads to two main disadvantages: (a) Bubbles decrease the amount of flat pieces of graphene that can be used for a quantum dot structure. (b) Deviations of the 2D-shape of a graphene sheet lead to local changes in the bandstructure. Next to that, application of large backgate voltages might electrostatically attract the bubble and flatten it, thereby changing the coupling with the gate.
   The solution to these problems include: (a) Search for graphene flakes that are long and small (e.g. 10 μm:1μm), we know from experience that such types of flake tend to contain little bubbles. This is most likely caused by the fact that bubbles tend to escape at the long sides and don't have the chance of getting large at all. (b) Perform the first transfer step (graphene on hBN) at a higher temperature of approx. 175°C. Although the Kim-group advised 70°C, we have performed transfers at 110°C as well and those certainly did not look worse. As the PMMA-film is very flexible (almost behaving as a liquid) at a temperature of 175°C, it could very well be that the graphene flake will have more freedom to land on the substrate in its natural 2D-shape. Another advantage would be that the alignment seems to be far more successful at this temperature (100% hit rate at 175°C versus approx. 60-70% at 70°C (including corrections for experience gained during this project)).

2. There is dirt on the graphene and the hBN-flakes as Fig. 3.6 and 4.14 show. For both the graphene and the hBN case, the dirt comes either from the tape used, or the PMMA film.

We tried to solve the tape-option by always taking new pieces of tapes for each transfer, but that did not seem to improve the situation a lot. It could still be that the dirt is just the glue from the tape; that won't be solved by taking new pieces, although less glue is expected to get transferred for a new piece. Instead of PMMA it might also be possible to use PDMS; A. Castellanos-Gomez (Low Temperature Laboratory of the Universidad Autonoma de Madrid (Spain)) reported that this did not leave residues but the yield of this process is low.
Next came the observation that annealing hBN flakes at 400°C seems to remove the dirt. This solution needs to be verified again, but unfortunately will only work for the bottom hBN-flake. The graphene and hBN coming from the PMMA film cannot be put into the annealing oven; the PMMA cannot withstand such temperatures for that duration. So to solve this problem a transfer-medium needs to be made that can withstand higher temperatures and allows the same transfer-functionality. A possibility could be Cellulose Acetate Butyrate (CAB) and it is being investigated at this moment.

Besides these two main problems, the following two points may need more attention in the future as well:

1. The interpretation of the Raman measurements. An example of something we do not yet fully understand is the Raman spectrum of the hBN-flakes. Almost all flakes show large number of counts over the whole spectrum. For some flakes this leads to an almost linear line (for counts versus Raman shift) with some spikes, whilst for others the spectrum more looks like a sinusoidal wave with several spikes. There is however also one flake that only shows spikes, and no significant continuous spectrum. Maybe these different type of spectra can also be used as a selection criteria for which hBN flakes to use.

2. In the present method water is used to separate the PMMA-film from the Si-wafer. The PMMA-film does not seem permeable to water (it's hydrophobic) and therefore we still call our transfer-method a dry-transfer method. If we might ever see evidence that water did get through, than one can decide to go to a method described in ref. [40]. They replaced the Aquasave layer with PVA which allowed mechanical peeling of the PMMA membrane without the need for exposing the graphene/PMMA substrate to a water bath, thereby achieving a fully dry transfer method. We tried this as well, but have not yet succeeded and in the meantime the Aquasave-method did work so we continued with that.

6.2.2 Future experiments

Apply a perpendicular magnetic field
When we have reached the phase of measuring Coulomb diamonds, it's possible to enrich the experiments by applying a perpendicular magnetic field. This kind of experiment has already been performed on monolayer graphene in ref. [13] and [41] and shows somewhat contradictory results. In [41] a ≈50 nm wide and ≈80 nm long QD has been made by etching. By applying a magnetic field the energy levels tend to move to the first Landau level with $E_0 = 0$, see Fig. 6.2 (a). The special thing about this measurement is that it allows you to precisely distinguish where the electron-hole crossover has taken place by just looking at the evolution of the position of your energy levels.
[13] have repeated the same experiment, only with a smaller dot (≈ 20 nm) and a different way of defining the edges (with AFM-etching). Their experimental result is depicted in Fig. 6.2 (b). This measurement also clearly shows a way to distinguish between the hole and electron regime, only the evolution of the energy-levels is different (in this case the energy goes up instead of down for larger B-field). The explanation Neubeck *et al.* give for the fact that their energy levels do not go to the zero Landau level is as follows: (1) Intravalley scattering is expected to be very efficient due to the rough edges of this dot which makes the electrons and holes 'forget' about their initial Dirac like spectrum and follow the standard behaviour for massive electrons and holes. (2) The magnetic length for the highest field of 14 T, $l_B = 7$ nm, which is comparable with the QD's $R =$

10 nm and therefore does not satisfy the condition for sufficiently high fields: $l_B \ll R$. In such a scenario the diagmagnetic shift of the first energy levels will be described by the theory from [42] (in which case the energy increases with B).
It will be interesting to check for us what kind of behaviour we get for our QD device (for a bilayer graphene the zero Landau level also lies at zero energy).

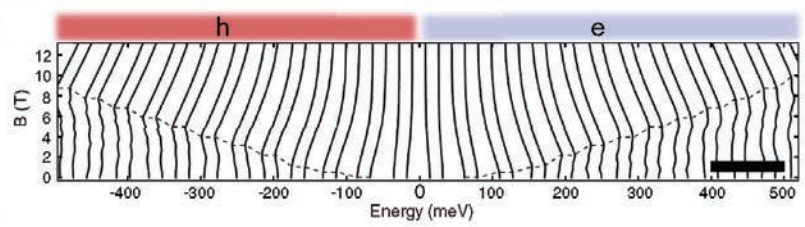

(a)

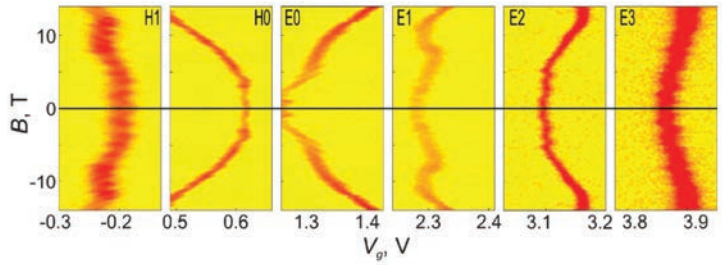

(b)

Figure 6.2: (a) Calculated levels of a graphene QD as a function of magnetic field. Zeeman splitting and a constant charging energy of 18 meV are included. Although these are theoretical calculations, they also see this in their experimental results [41]. (b) Evolution of the resonant-peak positions in a magnetic field from [13]. The figures with H0 and E0 show the evolution of the left and right part of $N = 0$ diamond respectively for V_{Bias}=0 V (T = 0.3 K). The conductivity varies from practically zero (yellow) up to 0.05 e^2/h (red).

Coupling multiple dots
If we want to implement these dots for quantum information processing, a register larger than one dot will be needed to perform any useful algorithms. This register of multiple dots can for example be created by a method described in ref. [16]. An example of a triple-quantum-dot set-up is shown in Fig. 6.3. Dot 1 and 2 are strongly coupled via cotunneling processes through the valence bands of barrier 2, barrier 3 and dot 2. The centre dot 2 is decoupled by detuning. The energy levels are chosen such that $\delta\epsilon_2 \ll \delta\epsilon_1$. This example shows that it is possible to strongly couple any two of the dots and decouple the other by detuning. This is only possible because the bandgap in graphene dots is small enough (in comparison to for e.g. GaAs) that the Fermi-level in each dot can be shifted from valence to conductance band and vice versa.

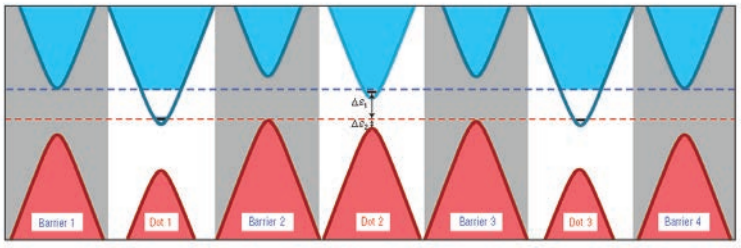

Figure 6.3: Triple-quantum-dot set-up [16], see text for details.

STM measurements on pseudo-magnetic fields
For the far future interesting STM-experiments can be thought of to measure pseudo-magnetic fields induced in certain shapes of bubbles [43]. Bubbles with a large height to width ratio and triangular shape are good candidates and can reach fields up to 300 T. Landau levels can be measured inside these bubbles and they will be spaced differently in energy for mono- and bilayers. This can serve as another test for the possible splitting of a bilayer inside a bubble, as suggested by Fal'ko (see section 4.2). But more importantly, these pseudo-magnetic fields have not yet been measured in bilayer graphene (only in monolayer).

Chapter 7

Acknowledgements

Time has gone fast and I think that I have only just started realising how lucky my situation in QT was. I have always been given the freedom to implement all the ideas I wanted to. One of the nicest things is that there are many intelligent people around willing to help and ready to shoot down my less brilliant ideas in a kind manner.

Special thanks go to my supervisor Stijn. You never gave me the idea that I did something terribly wrong, even when I ruined our first sample. This spirit is a vital quality for someone in experimental physics. In some way or another you also always quickly saw what kind of information was missing in my head to solve certain problems and understand articles. But I guess that the most important part for your successful role as a supervisor was your ability to laugh, I hope you won't forget Fred en Ria Onderbuik for a long time.

Lieven, I was honoured to be part of your team. I really appreciated the way you answer questions and are able to explain difficult physics to everyone around. I hope I'll ever reach the same amount of knowledge you have. You never gave me the feeling that you did not want to take the time for helping me with problems, and that stimulated me to keep thinking about the physics. The atmosphere during the meetings is also such that master students are given the feeling that they are a full member of the team.

Amelia, Mihai and Victor, thanks for helping me with all the machines needed for making the device and answering all my questions. Even though you did not have to supervise me, you always helped me in a nice way and thereby sped up my project.

I also want to thank all master's students for their graphene jokes. I guess I will remember the 'blijf je nog even plakken na je afstuderen' for a long time.

Last but not least I would like to thank my parents for the support they have given me during my studies and have always trusted me in making my own decisions.

Chapter 8

Appendix

8.1 Recipes and specific details for the dry-transfer method described in Chapter 3

This section provides details about the dry-transfer method from Chapter 3. It will be especially useful if you want to reproduce the steps and it contains hints on what can go wrong.

8.1.1 Step 1

Remarks for performing mechanical exfoliation
Mechanical exfoliation works in the same way for graphene and hBN. In both cases you start with a 'master-piece' of tape containing many graphite flakes or hBN crystals.

1. Get a new piece of blue Nitto tape and put this on top of the master-piece of tape. Rub against both pieces of tape for half a minute and pull the pieces apart. Continue with the new piece of tape.

2. Make a plastic window that fits the chip you are going to use. The dimensions should be such that there is a (square) hole inside that is 4-6 mm smaller in width than the actual chip (to ensure enough double sided tape can attach to the PMMA-layer). Around the hole should be $\pm$ 1 cm of plastic to ensure the window can float in water. Sandpaper the piece of plastic so that it cannot by accident rupture the PMMA-film with any sharp sides. Clean the plastic window with ethanol and next IPA.

3. Heat the chip to 100°C for 1-2 minutes so that any remaining watermolecules can evaporate.

4. Position the window on the chip and put the piece of tape on top of that. Be careful not to move the tape after it has hit the PMMA; in that case it will rupture anyway.

5. Press the tape softly with your finger to make it touch the whole chip. Next rub it really gently with the handle of a screwdriver for 2.5 minutes. Do not apply any pressure, just let the weight of the screwdriver do its task. If you rub for too long, a lot of glue from the Nitto tape might remain on the chip.

6. Now comes the most difficult part: getting the piece of tape off without rupturing the PMMA-film. For this you need a rectangular piece of plastic that just fits inside the square hole. You gently grab the piece of tape and under an angle of almost 90 degrees with the chip you slowly pull it off, whilst exerting pressure on the tape that is still on the chip with the rectangular piece of plastic.

7. After this step you should be finished and can start searching suitable flakes.

Recipe for making a Si chip covered by ±50 nm Aquasave and ±390 nm PMMA A6 950k

1. Put the chips in acetone and the ultrasound for approximately 3 minutes.
2. Repeat with isopropanol.
3. Rinse with distilled water.
4. Clean the chips further in 'Piranha' (150 mL 40% H_2SO_4 and 50 mL 30% H_2O_2) for at least 15 minutes.
5. Rinse with distilled water.
6. Dry the chips using the nitrogen-pistol.
7. Spin Aquasave for 5 sec. at 500 RPM and 55 sec. at 2000 RPM (± 50 nm).
8. Spin PMMA A6 950k for 5 sec. at 500 RPM and 55 sec. at 6000 RPM (± 390 nm).
9. Bake for 1-2 minutes at 140°C.

8.1.2 Step 2

The attachment of the plastic window to the chip was achieved by:

1. Putting double-sided tape on the sides of the window; this pieces of tape were approx. 4 mm wide.
2. Carving away a piece of the Aquasave and PMMA of the sides of the chip (less than 1 mm), so the water could more easily dissolve the Aquasave in the next steps.
3. Attaching the plastic window to the chip and placing them in water in such a way that the window floats (graphene side up).
4. Next the Aquasave will dissolve in approx. 10 minutes and the chip will be released leaving a layer of PMMA such as shown in Fig. 3.8 (b). If the chip does not release by itself you can gently take the plastic window out of the water and put the whole thing on a tissue. Take two tweezers: with one you can bend the plastic window and with the other you can keep the Si-wafer down: the two will release.

Remarks for performing transfers

- Check the position of your flake w.r.t. to the window. If it's really close to the sides, it will be difficult to reach it with the metal sphere from the microscope glass. Next to that, your hBN-chip might now need to be so close to the sides of the window as well, that they will hit and thereby misalign. It's ideal to have flakes at least 4 mm away from the sides of your window.
- To ensure that the plastic window does not touch the heater for the microscope during the transfer (and thereby leading to misalignment), one should put the chip on a small piece (1x1 cm) of metal approx. 3 mm high.
- The metal sphere from the microscope glass usually contains a lot of residues from previous transfers which can easily be seen under the optical microscope. Putting the microscope glass in a sonicator is not an option as this will break the glass. Leaving the glass in acetone for too long will dissolve the stycast (used to glue the metal sphere to the glass). It is therefore better to clean the inside of the sphere with a thin clean screwdriver and tissues with acetone.

- If you perform the transfer at high temperatures such as 175°C the plastic window will start bending after a while due to the heating. This makes the alignment more difficult. It is therefore best to first align the whole system at room temperature and get the orientation of the chip right. Next, remove the entire microscope (with the heater and chip on it) from under the plastic window and start heating to the desired temperature. After the temperature has been reached wait for another 2-4 minutes to make sure the whole system has fully expanded due to the heating. Now restore the microscope back under the plastic window and you'll only need to do a little adjustments to the alignment. This can be done quick enough to prevent severe bending of the plastic.

- Take your time for the alignment. You'll need to change the focus of the microscope from the chip to the flake being transferred quite often and changing the height of the chip also induces lateral movement (probably from the connection of the heater with electrical wires to the box outside the microscope). The absolute height changes I made while changing focus from one to the other, were approximately 2-5 mm to make sure the chip and flake don't hit each other by mistake.
  So check the alignment at least 3 times by focussing on the chip and back to the graphene/hBN flake again; if nothing changed during this time you can be quite sure it will all work out. It is really worth the effort.

Problems encountered during transfers
Several problems have been encountered during the transfer procedures. Problems include:

1. The PMMA-film is not so strong and if not treated carefully (e.g. moving the microscope glass when it is already attached to the plastic window) it will break. After some 'training' in transferring this problem occurs less often. Otherwise solutions would be to increase the thickness of the PMMA (keeping in mind the contrast values) or using round plastic windows instead of square ones to support the PMMA-film.

2. If the hBN-chip touches the plastic window when you bring the PMMA-film close to the hBN, it will lead to misalignment.

3. The plastic window could melt if the transfer takes too long with the heating on. After some training it is possible to perform the transfer quick enough, and otherwise one can use plastics that are resistent to higher temperatures.

8.1.3 Step 3 and 5

Step 3 and 5 involve the annealing of the chips in the nanotube oven located at the BioNanoscience department. The following steps were done to perform the annealing:

1. Put the tube in the oven, without connecting it to the argon and hydrogen cylinder. Heat the oven to 900°. Once it has reached this temperature, leave it there for at least 15 minutes to burn away any contaminations inside the tube.

2. Attach the argon and hydrogen cylinder in the correct way and let argon flow at 2.4 L/min for 5 minutes to remove any oxygen inside the tube. Next also open the hydrogen at 0.7 L/min and leave this open for another 5 min.

3. Close the hydrogen valve and keep the argon open. Set the oven to room temperature, open the lid, and let it cool down.

4. Once cooled down, close the argon valve and open one side of the tube. Place the samples, close the lid and flush again for 5 min. with argon gas (2.4 L/min).

5. Set the right temperature for the oven and let it heat up. Note: the oven has an overshoot of approx. 30°C; it's advisable to set the temperature first somewhat lower to not overheat your device. In the meantime you can open the hydrogen cylinder again at 0.7 L/min.

6. Once the baking time has been reached: close the hydrogen cylinder and turn down the heating. Let the samples cool down with the lid closed to ensure slow cooling and as little thermal stress as possible.

7. Once room temperature has been reached; close the argon cylinder and get the samples out.

8.1.4 Step 6

Here the same hints apply as given in section 8.1.2. Some extra remarks can be made:

- Think carefully about the orientation of the top hBN-flake with the sample. Not all orientations will be able to follow the shape of the source/drain contacts easily. You can really think of this system as a blanket falling down.

- If you misalign in this step and by accident withdraw the plastic window including the PMMA film you have a high risk of rupturing you graphene. The PMMA-film tends to stick really well to the graphene and hBN-flakes; so if it (instead of the hBN top flake) gets in contact with your graphene it is best to not get it off mechanically (by withdrawing) but just stop and dissolve the PMMA with acetone. Then check in the AFM and if everything is still fine: redo this transfer step.

A clear example of a misalignment problem is shown in Fig. 8.1.

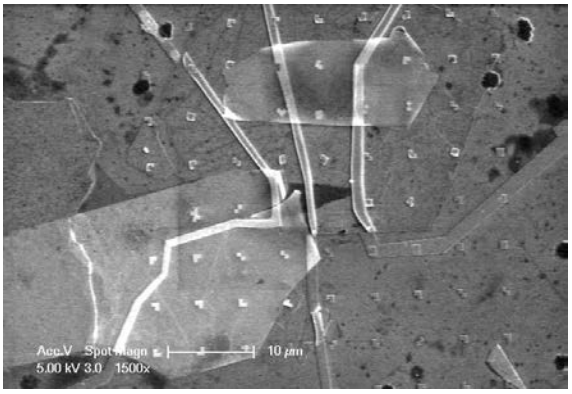

Figure 8.1: SEM-image of an example of misalignment during the second transfer step. The dark black area in between the electrode shows the graphene flake. The big light grey area on the left and the area in the middle-top are a hBN flake; they are both not on top of the graphene flake.

Bibliography

[1] L.P. Kouwenhoven. *Electron transport in quantum dots*. Kluwer, Alphen aan de Rijn, the Netherlands, 1997.

[2] K.S. Novoselov. Electric field effect in atomically thin carbon films. *Science*, 306:666–669, 2004.

[3] C.R. Dean. Boron nitride substrates for high-quality graphene electronics. *Nature Nanotechnology*, 5:722–726, 2010.

[4] P.R. Wallace. The band theory of graphite. *Phys. Rev.*, 71:622–634, 1947.

[5] L.D. Landau. Zur theorie der phasenumwandlungen. *Phys. Z. Sovjetunion*, 11:26–35, 1937.

[6] R.E. Peierls. Quelques proprietes typiques des corpses solides. *Ann. I. H. Poincare*, 5:177–222, 1935.

[7] E. McCan. Landau-level degeneracy and quantum hall effect in a graphite bilayer. *Phys. Rev.*, 96:086805, 2006.

[8] E. McCan. Assymetry gap in the electronic band structure of bilayer graphene. *Phys. Rev. B.*, 74:161403, 2006.

[9] E. Castro. Biased bilayer graphene: semiconductor with a gap tunable by the electric field effect. *Phys. Rev.*, 99:216802, 2007.

[10] A.H. Castro Neto. The electronic properties of graphene. *Reviews of modern physics*, 81:109–162, 2009.

[11] X.L. Liu. *Quantum dots and Andreev reflections in graphene*. PhD-thesis Delft University of Technology, 2010.

[12] J.B. Oostinga. Gate-induced insulating state in bilayer graphene devices. *Nature Materials*, 7:151–157, 2007.

[13] S. Neubeck. From one electron to one hole: Quasiparticle counting in graphene quantum dots determined by electrochemical and plasma etching. *small*, 6:1469–1473, 2010.

[14] Y.V. Nazarov. *Quantum Transport*. Cambridge University Press, New York, 2009.

[15] M. Nirmal. Observation of the "dark exciton" in cdse quantum dots. *Phys. Rev.*, 75:3728–3731, 1995.

[16] B. Trauzettel. Spin qubits in graphene quantum dots. *Nature physics*, 3:192–196, 2007.

[17] B.G.; Sanjay B. Streetman. *Solid State electronic Devices (5th ed.)*. New Jersey; Prentice Hall, 2000.

[18] C. Stampfer. Tunable graphene single electron transistor. *Nano Letters*, 8:2378–2383, 2008.

[19] J. Moser. Fabrication of large addition energy quantum dots in graphene. *Appl. Phys. Lett.*, 95:173506, 2009.

[20] D.A. Areshkin. Ballistic transport in graphene nanostrips in the presence of disorder: importance of edge effects. *Nano Letters*, 7:204–210, 2007.

[21] M. Wimmer. Robustness of edge states in graphene quantum dots. *Phys. Rev. B*, 82:045409, 2010.

[22] K.I. Bolotin. Ultrahigh electron mobility in suspended graphene. *Solid State Communications*, 146:351–355, 2008.

[23] private communication with A.M. Goossens.

[24] G. Giovannetti. Substrate induced band gap in graphene on hexagonal boron nitride: ab initio density functional calculations. *Phys. Rev. B.*, 76:073103, 2007.

[25] K. Watanabe. Direct-bandgap properties and evidence for ultraviolet lasing of hexagonal boron nitride single crystal. *Nature Mater*, 3:404–409, 2004.

[26] A.F. Youn. Electronic compressibility of gapped bilayer graphene. *arXiv:1004.5556v2*, 2010.

[27] S. Das Sarma. Conductivity of graphene on boron nitride substrates. *arXiv*, 2010.

[28] C. H. Chen. Intrinsic and extrinsic performance limits of graphene devices on SiO_2. *Nature Nanotech.*, 3:206–209, 2008.

[29] S. Fratini. Substrate-limited electron dynamics in graphene. *Phys. Rev. B.*, 77:195415, 2008.

[30] L.M. Malard. Raman spectroscopy in graphene. *Physics Reports*, 473:51–87, 2009.

[31] J.D. Jackson. *Classical Electrodynamics*. Wiley, 1975.

[32] R. Hanson. Zeeman energy and spin relaxation in a one-electron quantum dot. *Phys. Rev.*, 91:196802, 2003.

[33] B.E. Feldman. Broken-symmetry states and divergent resistance in suspended bilayer graphene. *Nature Physics*, 5:889–893, 2009.

[34] G.F. Schneider. Wedging transfer of nanostructures. *Nano letters*, 10:1912–6, 2010.

[35] P. Blake. Making graphene visisble. *Appl. Phys. Lett.*, 91:063124, 2007.

[36] S.J. Byrnes. Fresnel equation solver for multilayer thin films. *http://sbyrnes321.byethost11.com*, 2009.

[37] A.C. Ferrari. Raman spectrum of graphene and graphene layers. *Phys. Rev.*, 97:187401, 2006.

[38] T. Taniguchi. Synthesis of high-purity boron nitride single crystals under high pressure by using ba-bn solvent. *J. Cryst. Growth*, 303:525–529, 2007.

[39] E. Stolyarova. Observation of graphene bubbles and effective mass transport under graphene films. *Nano Lett.*, 9:332–337, 2009.

[40] C.R. Dean. Multicomponent fractional quantum hall effect in graphene. *arXiv*, 1010.1179v1, 2010.

[41] J. Guttinger. Electron-hole crossover in graphene quantum dots. *Phys. Rev. Lett.*, 103:046810, 2009.

[42] S. Tarucha. Shell filling and spin effects in a few electron quantum dot. *Phys. Rev. Lett.*, 77:3613–3616, 1996.

[43] N. Levy. Strain-induced pseudo magnetic fields greater than 300 tesla in graphene nanobubbles. *Science*, 329:544, 2010.